# Simulation, Design and Construction of a Gas Electron Multiplier for Particle Tracking

By

Andrej Sipaj

A Thesis Submitted in Partial Fulfillment

Of the Requirements for the Degree of

Master of Applied Science

In

Nuclear Engineering

Faculty of Energy Systems and Nuclear Science Program

University of Ontario Institute of Technology

December, 2012

# Abstract

The biological effects of charged particles is of interest in particle therapy, radiation protection and space radiation science and known to be dependent on both absorbed dose and radiation quality or LET. Microdosimetry is a technique which uses a tissue equivalent gas to simulate microscopic tissue sites of the order of cellular dimensions and the principles of gas ionization devices to measure deposited energy. The Gas Electron Multiplier (GEM) has been used since 1997 for tracking particles and for the determination of particle energy. In general, the GEM detector works in either tracking or energy deposition mode. The instrument proposed here is a combination of both, for the purpose of determining the energy deposition in simulated microscopic sites over the charged particle range and in particular at the end of the range where local energy deposition increases in the so-called Bragg-peak region. The detector is designed to track particles of various energies for 5 cm in one dimension, while providing the particle energy deposition every 0.5 cm of its track. The reconfiguration of the detector for different particle energies is very simple and achieved by adjusting the pressure of the gas inside the detector and resistor chain. In this manner, the detector can be used to study various ion beams and their dose distributions to tissues. Initial work is being carried out using an isotopic source of alpha particles and this thesis will describe the construction of the GEM-based detector, computer modelling of the expected gas-gain and performance of the device as well as comparisons with experimentally measured data of segmented energy deposition.

# Table of Contents

# Acknowledgment

First, I would like to thank Dr. Anthony Waker for his constant support and encouragement in my research and the writing of this thesis. I sincerely appreciate his guidance and support during the period of this work and most of all, his patience and understanding.

I would like to thank to Dr. Heinrich Schindler for his help, patience and time with the Garfield++ simulation problems that I faced and to Fawaz Ali for his MCNPX model contribution.

I would also like to thank all my professors, colleagues and friends who gave me generous support throughout my time at UOIT.

I am grateful to the University Network of Excellence in Nuclear Engineering (UNENE) and the Natural Science and Engineering Council of Canada (NSERC) for their financial contributions to this project.

Lastly, I am thankful to my family, especially my parents, Frantisek and Helena Sipaj, and my sister, Katarina Sipaj for helping me through the difficult times and for being a source of inspiration during the course of my research and throughout my university education.

# List of Figures

# List of Tables

# Nomenclature

| | |
|---|---|
| $\vec{E}$ | Electric Field (V/cm) |
| E | Energy (MeV) |
| $G$ | Gain |
| $P$ | Pressure (Torr) |
| $S$ | Stopping Power (MeV/mm) |
| $V_D$ | Drift Region Voltage Drop (V) |
| $V_{GEM}$ | GEM Region Voltage Drop (V) |
| $V_I$ | Induction Region Voltage Drop (V) |
| $\rho$ | Density (g/cm$^3$) |
| $X_D$ | Thickness of Drift Region 1.3 (mm) |
| $X_I$ | Thickness of Induction Region 9.1 (mm) |
| $\sigma$ | Cross Section (barn) |
| $v_d$ | Drift Velocity (mm/sec) |
| D | Diffusion coefficient |

# Acronyms

| | |
|---|---|
| GEM | Gas Electron Multiplier |
| HVS | High Voltage Supply |
| LLD | Lower-Level Discriminator |
| MCA | Multi Channel Analyser |
| MCNPX | Monte Carlo N-Particle eXtended |
| MWPC | Multi Wire Proportional Counter |
| PCB | Printed Circuit Board |
| PRR | Proton Range Radiography |
| RT | Radiation Therapy |
| SRIM | Stopping and Range of Ions in Matter\ |
| ULD | Upper-Level Discriminator |

# 1 Chapter

## 1.1 Introduction

Since the discovery of x-rays by Wilhelm Rontgen in the 1895 [1], the development of various kinds of radiation detectors began to play a key role in describing and analyzing different properties of radiation and interactions with matter. Initially, the detectors where only capable of counting the number of particles passing through the detector and measuring radiation particle energy, as of today complex Time Projection Chamber detectors are capable of tracking a single low energy electron its velocity and measuring the energy that is being deposited at any point of the particle track.

The evolution of radiation detectors starts with J. J. Thomson's detector just a few months after the initial discovery of the unknown x-rays [2]. Even though the design was relatively simple, an ion chamber that has one positive and one negative flat electrode separated by air, and the readings from the chamber were obtained by measuring the current cross the two electrodes, it provided major discoveries and the fundamentals of radiation interactions with matter. Some of the major findings were that the air, normally an isolating material, can turn conductive when a radiation particle passes though the detector sensitive volume, and that by increasing the voltage drop across the electrodes increases the number of electrons that are being collected up to certain point after which the number stays constant.

The observation of John Townsend, that a significant increase in an ion chamber's current is produced at reduced gas pressures when the high voltage is increased well beyond that at which the saturation current is reached, led to the invention of the first counting tubes (today known as proportional counters) by Rutherford and Hans Geiger in 1908 [2]. Townsend's explanation was that the increased velocity of the electrons traveling to the collecting electrode permitted them to ionize the air molecules. It was this additional ionization that produced pulses large enough to be counted. Shortly after the invention of the proportional counter the voltage across the electrodes have been increased even further what gave a base for the creation of Geiger Mueller tubes with one large pulse in 1928.

Even though the possibility of light output from a barium platinocyanide screen when exposed to X-rays has been know since the 1895, it was not until the Manhattan Project that activities contributed to the development of new kind of radiation detector, the scintillator detector, in 1944 [3]. Around the same time, Bell Laboratories invented the semiconductor detector that uses the reverse biased p-n junction to detect alpha particles [4].

From these times, independent of the size, shape and purpose of any radiation detector, all detectors can be divided into three main groups. Gas filled detectors, solid state detectors and scintillation detectors. Radiation detectors in general have been continuously improving and developing since these early times by studying the same basic principles that were discovered and used in these first detector prototypes.

During more recent years (1968), the invention of the Multi Wire Proportional Counter (MWPC) at CERN stands out in gas detector development [5]. The MWPC provided a breakthrough in particle detection as it is capable of both particle tracking and energy reading. For this reason, the inventor Georges Charpak was awarded the Nobel Prize in Physics in 1992. However, the signal from MWPC is extremely low for low energy particles and could not be picked up by data acquisition systems. The problem initiated the search for a new device that could multiply the signal (the electrons from primary ionizations) prior to the MWPC. As a result for this given need the Gas Electron Multiplier (GEM) was invented [6].

## 1.2 Gas Electron Multiplier

The Gas Electron Multiplier (GEM) is a relatively new concept of particle detection which was invented by Fabio Sauli in the 1997 at the Gas Detectors Development Group (CERN). The initial idea was to create a component that would help to increase electron gain in a Multi-Step Chamber before entering the main detecting element which at that time was the Parallel Plate and Multi-Wire Proportional Counter in order to detect a single low energy photon. With rapid improvements of the production techniques over the first few years the initial gain of 10 increased to the order of $10^4$ [7], [8], [9]. With the high gains, current detection systems no longer needed a proportional counter collection system but instead printed circuit collection plates can be sufficient for certain situations.

A typical GEM foil consists of two 5 µm thick layers of copper that are separated by 50 µm kapton foil [10]. The kapton is a plastic material with high resistivity ($10^{11}$ Ω/mm) and dielectric strength (126 kV/mm) that can be produced at extremely small thicknesses [11]. The foil is chemically pierced by a high density pattern of holes, from 50 to 100 holes per $mm^2$ based on needs while each hole has a bi-conical shape, see Figure 1.1. Currently, the area of GEM foils produced at the CERN ranges from 25 $cm^2$ up to a 1000 $cm^2$ [10].

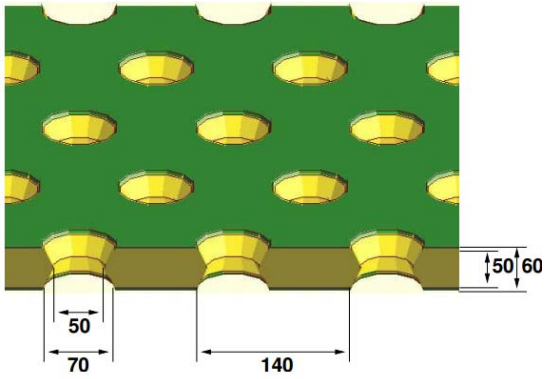


Figure 1.1: Drawing of typical GEM foil with dimension is micrometers [12]

In general, all GEM detectors work with the same principle. The system consists of a drift field where all the initial gas ionization takes place. One of the GEM copper layers acts as an anode and one external electrode acts as a cathode. The drift should operate as an ion chamber where no recombination of the newly created ion-pairs can occur. The electrons from the ion-pairs drift towards the anode, the GEM foil, and the electric field that is being created around the GEM holes redirects the electrons to the holes rather than to the copper metal. The electric field around the GEM is created by applying different voltages between the two layers of copper. The shape of the field

mainly depends on the applied voltage and the shape of the holes. Since the geometry of all holes and the voltage across the GEM is uniform, the electric field within each hole is uniform. As the dimensions of the foil are extremely small in the order of micrometers, potentials up to 100 kV/cm are possible within a normal range of the GEM operation where the potential of 100 to 650 V is applied based on the needs of the electron pre-amplification [9]. Each of the holes acts as a small proportional amplifier while the stability of the gain is obtained by compact size of amplification region.

On exit from the GEM the created electron avalanche is forced to drift towards the induction region where, similar to that drift region, an external electrode, acting as an anode, is added to guide the electron to the collection system. The induction region should also operate in the ion chamber region therefore, no additional electron multiplication can occur, in order to sustain the stability of the overall gain of the system. The Figure 1.2 shows lines of electric field distribution in red and equipotential lines in blue. The drift is located above and induction region bellow the GEM.

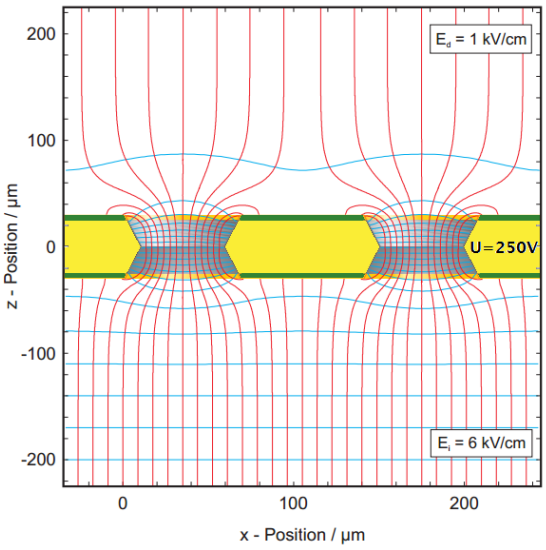


Figure 1.2: Simulated field settings of a GEM [12]

## 1.3 Thesis Objective

Proton Therapy is a type of particle therapy which uses a beam of protons to irradiate diseased tissue or tumour for treatment of cancers. In contrast to the traditional radiotherapy such as photon or electron treatment, the energy deposited increases near the end of the particle track (in Bragg peak) while the beam has a finite depth. Therefore, the healthy cells that are located before the tumour cells (from beam direction) receive a lower dose and the healthy cells behind receive no or very small dose. Overall, the main advantage of proton therapy is that it enables the treatment of tumours with a dose distribution that spares healthy tissues or prevents damage to sensitive tissues in proximity to the tumour.

The energy deposition, stopping power, of the proton beam must be precisely known and tested in order to deliver the highest dose to a specific location. The tests are done with Proton Range Radiography (PRR) that consists of range telescope made

with a stack of scintillators [13]. As the beam passes perpendicular through the stack it deposits its energy into each scintillator at different depth. This kind of device could be replaced by GEM detector that can directly track the energy distribution of the proton beam to very precise locations.

Particle tracking is also important in building discriminating detectors that can measure low energy beta particles from tritium against a background of longer range electrons from gamma-rays, which is a problem of particular significance in CANDU power plant radiation protection.

For these reasons, the main objective of this thesis is to construct a simple GEM to test and understand the performance of these devices for particle tracking and energy measurements. For simplicity, the charged particle was chosen to be a 5.5 MeV alpha particles from Americium-241.

A secondary objective of this work was to provide a general guidance manual for the construction of GEM detectors which uses PCB as a collection electrode since the GEM foils are a relatively new concept in radiation detection and there is interest in looking for possible new applications for this kind of device.

## 1.4 Past Trials of GEM Detectors for Tracking and Energy Measurements

Understanding tracking and stopping power experiments conducted with GEM detectors in the past is essential to developing a good detector understanding as well as understanding the properties governing how a heavy charged particle interact with

matter. Since the direct stopping power measurements with GEM detectors that uses PCB collection board have not been done, findings from two papers are combined to provide a general working principal and the feasibility of using the proposed detector.

The prospect of tracking alpha particles which travel parallel to the GEM foil is shown in a luminescence and imaging paper with gas electron multipliers [7] which describes a detector that has been built by collaboration of Laboratório de Instrumentação e Física Experimental de Partículas, LIP-Coimbra and the Physics Department of the University of Coimbra. This double GEM detector does not use a PCB collection board but instead the CCD camera that detects photons that are emitted by $CF_4$ scintillation. The detector is capable of detecting a single alpha particle from Am-241 and its Bragg peak in form of light intensity as shown below.

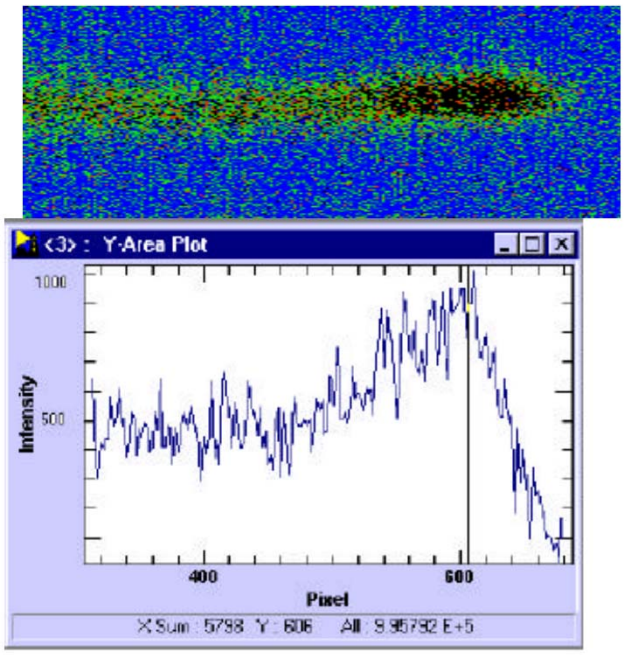


Figure 1.3: Resulting image of a single alpha particle by GEM scintillation using gas $Ar/CF_4$ (95/5)

The initial GEM detectors needed a MWPC in order to obtain position or energy read out due to the low gain obtained by the GEM foil. However, as the production technology of GEMs improved, MWPC have been replaced by simple PCB read-out boards. One of the first examples that uses one large collection plate, that is segmented into 200 µm stripes while all segments are still connected together for a GEM + PCB is presented in Further Development of the Gas Electron Multiplier report [14]. The GEM detector in this case has sufficiently high gain for the pre-amplifier to picked up signal and provide good energy resolution

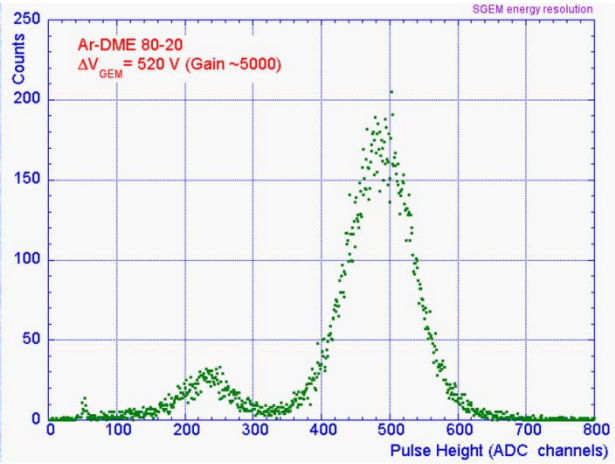


**Figure 1.4: Energy resolution of single GEM with single PCB readout board, FWHM ~18% at 5.9 keV**

Combing knowledge of these two papers suggest that it is possible to build a tracking detector that not only tracks an alpha particle that travels parallel to the GEM detector but also obtain the alpha particle energy by PCB collection board.

## 1.5 Outline of Thesis

This thesis will cover the principles of alpha particle energy deposition in a medium, the ionization multiplication processes, the effects of various electric fields on

the avalanche based on which, an Am-241 detectors will be built. Chapter 2 will cover the background to the properties of alpha particles mainly their interactions with matter and electron multiplication properties such as Townsend coefficient, penning transfer, electron drift velocity, diffusion coefficient and electron attachment. Moreover, an introduction to the simulation software used will be given. Chapter 3 explains the physical design of the GEM detector where each part of the detector (sensitive volume, collimator with window, pre-amplifier and its board, voltage and current divider and the collection plate switch) is discussed in detail while physical dimensions of the detector are also provided. The selection of the multiplication gas and the required pressure for the given system can also be found here. Chapter 4 is dedicated to simulation of the electron avalanche. The results of the simulation help to understand the general properties of the GEM detector under various conditions and help to select ideal settings for the proposed detector. Chapter 5 will discuss results from a constructed prototype. The results for Am-241 stopping power are shown and compared to a basic MCNP model. The conclusion in Chapter 6 will summarize research methods and the development of the techniques over the course of this investigation. Moreover, future development and improvements of the system as well as future use for the proposed detector will be addressed.

# 2 Chapter: Background and Theory

## 2.1 Background and Theory of Charged Particle Energy Loss in Gases

### 2.1.1 Ionization by Alpha Particles

As an alpha particle travels through matter, it causes ionization and excitation of the atoms of the material irradiated. Both of these processes result mainly from the Coulomb force as the alpha particle charge pulls the electron from its origin. Depending on the proximity of the encounter, this impact due to the Coulomb force may be sufficient either to raise the electron to a higher laying shell within the absorber atom (excitation) or to remove the electron completely from the atom (ionization) [15]. Therefore, a charged particle that traverses the gas of a drift chamber leaves a track of ionization along its trajectory. The energy that is transferred to the electron must come from the energy of the alpha particle, therefore the velocity of the latter decreases.

As the encounters with the gas atoms are purely random, they can be characterized by a mean free flight path, which is commonly denoted as $\lambda_i(\varepsilon)$. The mean free flight path between ionizing encounters is given by the ionization cross-section per electron $\sigma_i(\varepsilon)$ and the number density n of electrons [16]:

$$\lambda_i(\varepsilon) = \frac{1}{n\sigma_i(\varepsilon)} \tag{2.1}$$

From the definition above, it follows that the mean free flight path of the alpha particle (and ultimately its range) can be simply changed by adjusting the density or pressure of the gas.

As the maximum energy that can be transferred by a single collision is $4Em_0/m$, where the $m_o$ is rest mass of an electron and m the mass of the alpha particle, the alpha particle must collide many times before reaching thermal equilibrium ($m_0 << m$).

### 2.1.2 Stopping Power

As discussed before, an alpha particle can lose its energy only by ionization and excitation of molecules along its track. This loss is not linear due to the change of velocity and particle charge. Therefore, the concept of stopping power has been introduced in order to characterize the rate at which a charged particle loses its kinetic energy. The energy loss as a function of particle energy and atomic number is given by the Bethe-Bloch-formula [17]:

$$|S| = \frac{dE}{dx} = \frac{4\pi Z_{eff}^2 e^4 n_e}{m_e v^2} \ln\left(\frac{2mv^2}{< I > (1-\beta^2)}\right) + \ (higher\ relativistic\ turms) \tag{2.2}$$

where $n_e$ is the number density of the electrons of the target material, $e$ is the elementary electric charge, $m_e$ is the electron mass, $v$ is the particle velocity, $\beta$ is the particle velocity in units of speed of light, m is the mass of projectile and *<I> is* the mean ionization potential of the atoms in the stopping medium, and $Z_{eff}$ is the effective charge empirically approximated by Barkas [18]. At high energies, all projectiles are stripped of their electrons and the effective charge equals to the atomic number. At small energies (close to the end of the trajectory – Bragg peak region) electrons are collected from the target atoms and the effective charge of the projectile decreases,

becoming close to zero when the particles stop. The change of $Z_{eff}$ is the main reason for the sharp decrease of the energy loss at lower energies [19]. As the rest of the variables in the equation are relatively constant, the initial increase of the stopping power is primarily due to the velocity decrease of the particle as a result of the energy loss. The rate at which the alpha particle loses its energy can be best shown by the Bragg curve. Initially the particle loses energy at lower rates, and then at significantly higher rates near the end of its track (creates the Bragg peak) and then the rate of energy loss drastically decreases at the very end of particle track.

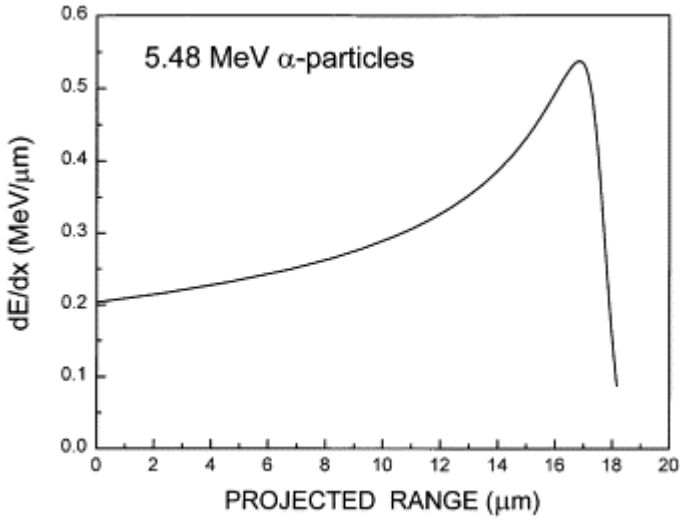


Figure 2.1: Example of Bragg curve [20]

### 2.1.3 Electron Multiplication in Gases

Electron multiplication is based on the mechanism of an electron avalanche. At increasing electric fields, the energy distribution of the drifting electrons extends beyond the thresholds of inelastic collisions, resulting in excitation and ionization of the gas molecules. In excitation, the molecules initially gain extra energy from electron

collisions and afterwards release the additional energy in the form of a photon until they reach their ground state. During the ionization process an electron produces an electron-ion pair and the two electrons, original and one from the pair, can cause further ionizations. The number of electrons hence grows exponentially with time until all electrons are collected at the anode.

The probability for an electron of energy $\varepsilon$ to create an ion pair depends on the ionization cross-section $\sigma_i(\varepsilon)$. Under the assumption that the ionizing collisions are independent of each other, the mean free path for ionization $\lambda_i$ relates to the cross-section given in equation 2.2 [16].

The mean number of ionizations per unit length is called the Townsend coefficient or collisional rate and is defined as:

$$\sigma(\varepsilon) = 1/\lambda(\varepsilon) \tag{2.3}$$

In practice, it is more helpful to know the Townsend coefficient at a given value of the electric field E and $\sigma(\varepsilon)$ should be integrated over the electron energy distribution $\mathrm{p}(\mathrm{E}, \varepsilon)$:

$$\sigma(\mathrm{E}) = \int_0^\infty \mathrm{p}(\mathrm{E}, \varepsilon)\sigma(\varepsilon)\, \mathrm{d}\varepsilon \tag{2.4}$$

The multiplication factor, or gain, can be calculated from the Townsend coefficient. Let N(x) be the number of electrons present in the avalanche after a drift over a distance x along the field E(x). After a path dx, the increase of the number in electrons is proportional to N(x) and dx [16]:

$$dN = N(x)\sigma\big(\mathrm{E(x)}\big)\mathrm{dx} \tag{2.5}$$

with σ(E(x)) being the Townsend coefficient at the field experienced by the electrons over the path dx. After a distance Δx = $x_1$-$x_0$, the avalanche size is obtained by integrating the previous equation:

$$\mathrm{N}(\Delta\mathrm{x}) = \mathrm{N}_0 \mathrm{e}^{\int_{x_0}^{x_1} \sigma(\mathrm{E(x)})\,\mathrm{dx}} \tag{2.6}$$

where $N_0$ is the number of electrons at $x_o$. The gain in an arbitrary field configuration can be simply expressed as:

$$\mathrm{G}(\Delta\mathrm{x}) = \mathrm{N}(\Delta\mathrm{x})/\mathrm{N}_0 = \mathrm{e}^{\int_{x_0}^{x_1} \sigma(\mathrm{E(x)})\,\mathrm{dx}} \tag{2.7}$$

### 2.1.4 Penning Transfer

The actual electron multiplication in gas based detectors sometimes far exceeds the gain calculated using the Townsend coefficient alone. The most notable case is when a gas with a low ionisation potential is added to a gas with higher-energy excitation states. The additional gain is accounted for by the transformation of excitation energy into ionisations:

$$A^* + B \rightarrow A + B^+ + e^-$$

The Townsend coefficient must be therefore corrected by the Penning transfer coefficient:

$$\sigma_{\mathrm{eff}}(\mathrm{E}) = \sigma(\mathrm{E})\left(1 + \mathrm{r}\frac{\mathrm{v_{exc}}}{\mathrm{v_{ion}}}\right) \tag{2.8}$$

where r is the probability that an excited state is transformed to an ionised state while $v_{exc}$ and $v_{ion}$ are the excitation and ionisation frequencies (collisions per time interval, generally in MHz) [21]. These frequencies are defined by the mean free path of the particle and its drift velocity for both ionizations and excitations of the molecules of the gas.

### 2.1.5 Drift Velocity of Electrons

The force on a charge q moving with velocity $v_d$ in the presence of an electric and magnetic fields of strength E and B, respectively, is given by the Langevin equation [16]:

$$F = m\frac{dv_d}{dt} = e\overrightarrow{(E + v\ x\ B)} - \overrightarrow{Q(t)} \tag{2.9}$$

where $\overrightarrow{Q(t)}$ is the friction force or stochastic force resulting from collisions. When applying constant electric filed and no magnetic field (B=0) the electron does not change its drift velocity ($\frac{dv_d}{dt} = 0$) due to constant scattering. For this reason, the Equation 2.9 at constant electric field without magnetic field can be rewritten as $\overrightarrow{Q(t)} = e\vec{E}$. Since $\overrightarrow{Q(t)} = \frac{m}{\tau}v_d$, when $v_d$ (the drift velocity) is constant and no magnetic field is applied the equation can be futher simplified to:

$$v_d = \frac{e\tau}{m}E \tag{2.10}$$

where τ is the mean time between collisions, given as $\frac{1}{n\sigma_s(\varepsilon)v_d}$,

When taking into account the balance between energy acquired from the electric field and collision losses, drift equation has to be changed to:

$$v_d{}^2 = \frac{eE}{mn\sigma_s(\varepsilon)}\sqrt{\frac{\lambda(\varepsilon)}{2}} \tag{2.11}$$

to include $\lambda(\varepsilon)$ in an elastic collision term (mean fraction of energy lost by an electron). The derivation of this equation can be found in Particle Detection with Drift Chambers [22].

### 2.1.6 Diffusion of Electrons

When electrons drift though a gas under the influence of magnetic or electric field, they do not strictly follow the field lines as they scatter with gas molecules. The electrons scatter almost isotropically in space in a direction of random motion after each collision, and diffuse transversally. However, they still generally following direction of the field lines in longitudinal diffusion.

Assuming a Gaussian distribution function for electrons, the diffusion coefficient can be obtained from the continuity equation for electron current in the following form [23], [24]:

$$D = \sqrt{\frac{2D_c}{\mu E}} = \sqrt{\frac{4\varepsilon}{3eE}} \tag{2.12}$$

The $D_c$ diffusion coefficient comes from the current continuity equation and the $\mu$ stands for the mobility of the gas.

### 2.1.7 Electron Attachment

Electron attachment is a side effect of the electron drift processes. This process must be controlled in order to preserve significant signal over noise as the negative ions

travel significantly slower than the electrons [25]. In general, electron attachment is a process where a free electron can attach to a molecule of gas and create a negative ion of this molecule or its fragments. The probability of the attachment is given by the electron cross-section at given energies. The process of electron attachment is shown below:

$$e^- + AB \rightarrow AB^{-*} \rightarrow A + B^-$$

where, AB is a diatomic or polyatomic molecule and A and B are fragments that can be either a single or molecular radical. Dissociative electron attachment is energetically possible if fragment B has a positive electron affinity and can form a stable negative ion. As the total energy of the reaction is positive, the transient ion $AB^{-*}$ is unstable. It can be stabilized by autodetaching the extra electron (elastic or inelastic electron scattering) or by dissociating thus transferring its excess energy to the dissociation process [26].

## 2.2 Background to Computer Simulation Software

### 2.2.1 Garfield++

Garfield++ is a computer simulation tool kit that was developed at CERN in 1984 by Rob Veenhof as there was a need for simulation of complex MWPC and micro-pattern drift chambers. The tool kit allows the user to not only track some primary particles but also secondary particles, due to its implementation of various software such as Magboltz (calculates properties of gases) and Heed (simulate ionisation of gas

molecules). Moreover, the program can simulate the behaviour of the particles under the influence of either electric or magnetic fields.

The program itself can only calculate electric or magnetic field distributions for flat plate or wire geometries. Therefore, description of fields generated in more complex geometries (like the GEM) must be imported from other software like Ansys, Elmer (freeware was used in this work) and CST. The general rule is to pick a simple building block that can be replicated to create the whole geometry, as it significantly speeds up the calculation times by reducing the number of nodes. The building block for a basic GEM detectors is shown below:

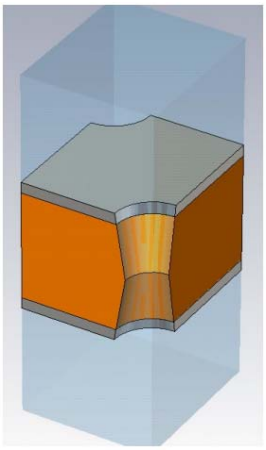

Figure 2.2: Basic building block of a GEM detector

The treatment of electron transport in gases is done by the Magboltz software which is part of the Garfield++ toolkit. All necessary parameters such as energy, drift velocity and diffusion are calculated here, by the use of its electron cross section databases and the equations presented in the previous section. In case of ion transport

properties, the tool kit cannot calculate ion mobility in gases and therefore the mobility must be also imported manually.

Moreover the new version, Garfield++ (GARFIELD is the original) was rewritten in the more common C++ language and built on the ROOT platform which allows the user to easily view the drift lines of electrons and ions, and also to do basic filtration of data by adding user-made functions to the final code. The example of the running code with running instructions can be found in Appendix A.

As previously mentioned, Garfield++ tool kit includes Heed software which generates ionization patterns of fast charged particles. The core of Heed is a photo-absorption and ionization model. It also provides atomic relaxation processes and dissipation of high-energy electrons. However, the program does not support tracking of alpha particles, and therefore, full simulation of the detector with this tool kit is not possible.

### 2.2.2 Gmsh and Elmer

As previously said, the Garfield++ is not capable of calculating more complex geometries of electric field and therefore software packages Gmsh and Elmer have to be used. The Gmsh is a CAD tool that creates geometries and provides some post-processing features like meshing. In order to create the structure of electric field the mesh is imported to Elmer, which is an open source multi-physics simulation software that includes physical model electromagnetism. The electric field is solved by partial differential equations which Elmer solves by the Finite Element Method. As the

programs in Linux can be interconnected, one script can be used to create field files needed by Garfield++ as the user sets the geometry and applied voltage to electrodes simultaneously.

### 2.2.3 Maxwell

The Maxwell program is a combination of Gmsh and Elmer and it has a full graphical interface that allows the user to study the electrical fields visually. Moreover, the program can work in 2D mode and show the field vectors and create equipotential lines at any location which is highly convenient when only small changes are done to the structure of the field. However, the program is only compatible with the old version of GARFIELD and not with Garfield++.

# 3 Chapter: Physical Design and Settings of the Detector

The topic of radiation detection is very wide and involves multiple variables that can be investigated (e.q. the type of particles to be detected, their energy, etc.). Therefore, every detector must be built for a very specific purpose. Following this approach, the detector proposed in this work is designed to read energy deposition values from an Am-241 source. Moreover, the main focus is on obtaining a clear and high signal when compared to the noise.

All single PCB GEM detector systems consist of three main parts: drift electrode, GEM foil and Induction electrode. However, the properties of the electrical fields, such as strength, size and shape, created in the system must be set correctly in order to make the detector work while the optimization of the system increases the signal to noise ratio as well as the probability of detection.

The general design can be divided into a number of main parts; vacuum chamber, sensitive volume, voltage divider, collimator with window (as the alpha source is isotropic), main board with pre-amplifier and collection plate switch. The schematic below represents the main structure of the detector. The green box represent the voltage divider, red the sensitive volume, yellow the collimator, blue the collection plate switch and black the main board with pre-amplifier.

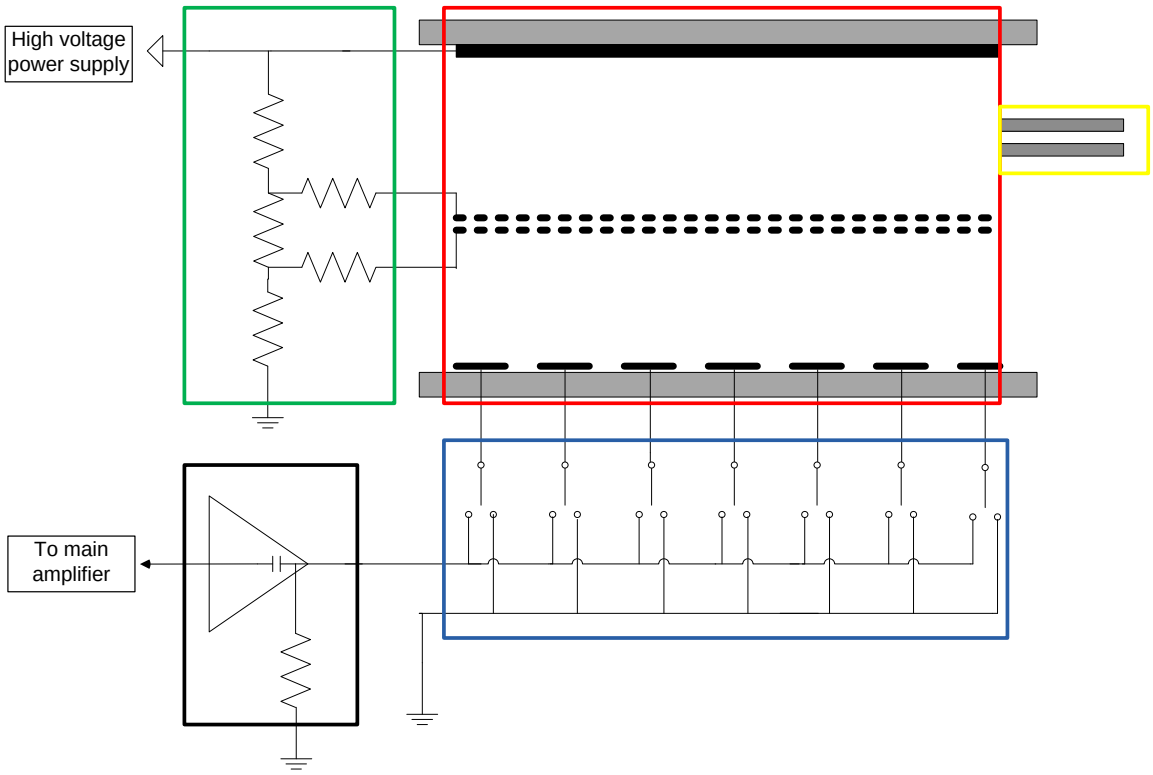


**Figure 3.1: General schema of GEM detector for the measurement of charged particle energy deposition track stucture**

## 3.1 Sensitive Volume

The sensitive volume is the most important part of the detector since the alpha particle undergoes ionization in this region while the electron multiplication and electron collection take place here as well. The system consists of only two segments the drift and induction regions that are defined by the GEM foil, drift and induction electrodes if the GEM electric field is not considered.

The initial ionization and transport of created electrons requires a high electric field of the order of few kV/cm, therefore the drift and induction fields must be relatively high. As the electric field between the electrodes is directly proportional to the voltage drop cross the electrode and inversely proportional to the spacing of the

electrodes, the high fields can be obtained by utilizing a small $d_d$ (thickness of drift field) and $d_i$ (thickness of induction field) while applying a voltage difference between them. Moreover, smaller $d_d$ and $d_i$ values improve the spatial resolution and reduce electron absorption due to attachment as the electrons have to travel shorter distances. For these reasons the $d_i$ is set to 1.3 mm, GEM frame is set to 0.6 mm and a spacer is set to 0.7 mm since only a small space is required for collection plate cable connections. However, since the selected alpha particle source (Am-241) is isotropic collimation of the source is necessary in order to create a narrow beam that could fit between the drift plate and GEM foil. A $d_d$ of 9.1 mm is selected as the most reasonable value when using a 28 mm collimator with 2 mm diameter bore and considering the fact that scattering of the alpha particle is not taken into account. If the scattering of the alpha particle would be considered then $d_d$ would need to be three times bigger, and this would require three times higher voltage drop, in order to keep the same intensity of the electric field.

The area of the sensitive volume is given by the size of the GEM foil, 50 X 50 mm in our case. The drift and induction electrodes are of the same size located directly below and above the GEM respectively, in order to create uniform field. The drift electrode is made out of a solid copper plate, while the induction (collection) electrode has 10 individual segments with 4.8 mm width each that are spaced by 200 μm as showed in figure below. The alpha particle track is represented by the arrow. This allows the user to pick either an individual segment or the whole plate for detection.

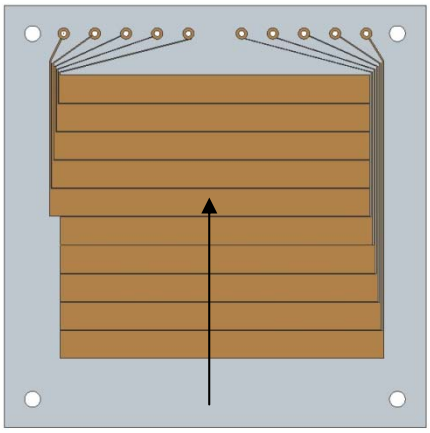

Figure 3.2: Image of segmented collection plate

## 3.2 Entrance Window with a Collimator

The detector is designed to detect an alpha source from outside of the vacuum chamber, this means that a user is not required to open the detector and place the source inside in order to run an experiment. The window is made out of 13 µm polyethylene terephthalate that is glued by epoxy resin to a bronze NPT fitting with a small 3 mm hole in middle. In case of window breakage, as the material is extremely thin and must withstand full atmospheric pressure across when under vacuum, the NPT fitting can be unscrewed and fully replaced. The window is placed 2.7 mm inside the fitting due to the mounting mechanism while the radiation source is not damaged by its surface touching anything. The teflon collimator is mounted directly to the NPT fitting reaching all the way to the sensitive volume of the detector as shown on the figure below (dimensions are not scaled). The diameter of the collimator is chosen to be 2 mm to collimate the isotropic source to a beam of maximum 9.1 mm thickness.

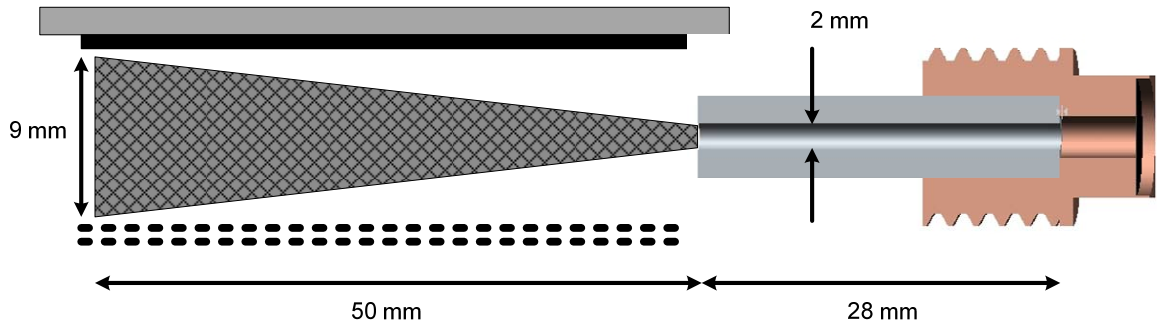


Figure 3.3: Schematic of collimation and collimator with dimensions

## 3.3 Main board with Pre-amplifier

As the expected signal from the collection plate of the detector is very small, the pre-amplifier is placed inside of the vacuum chamber which also acts as a Faraday cage. By doing so, the noise from outside of the chamber in the form of electromagnetic waves does not contribute to the detector signal.

A charge sensitive pre-amplifier is required to detect energy deposition by the collection of charge with good resolution for charged participle spectroscopy. For this reason, the Cremat CR-110 charge sensitive pre-amplifier was chosen since it has the highest gain in its class (1.4 volts /pC) in order to obtain a stable and high signal from the detector. Moreover, the compact size (22 X 23 X 3 mm) allows it to be placed within the prebuilt vacuum chamber, while still being mounted on top of the main board. The main board Cremat CR-150 AC provides stable AC coupling to the detector while it is directly compatible with the 8 pin pre-amplifier and provides all electronics for proper operation of the pre-amplifier chip (such as stable power supply to prevent fluctuation of the gain) and input capacitor. An older version (version 5) of the board is used as it is

significantly smaller than the newer versions. On the other, hand it does not contain an input for a test pulser. The diagram of the pre-amplifier connection is presented below.

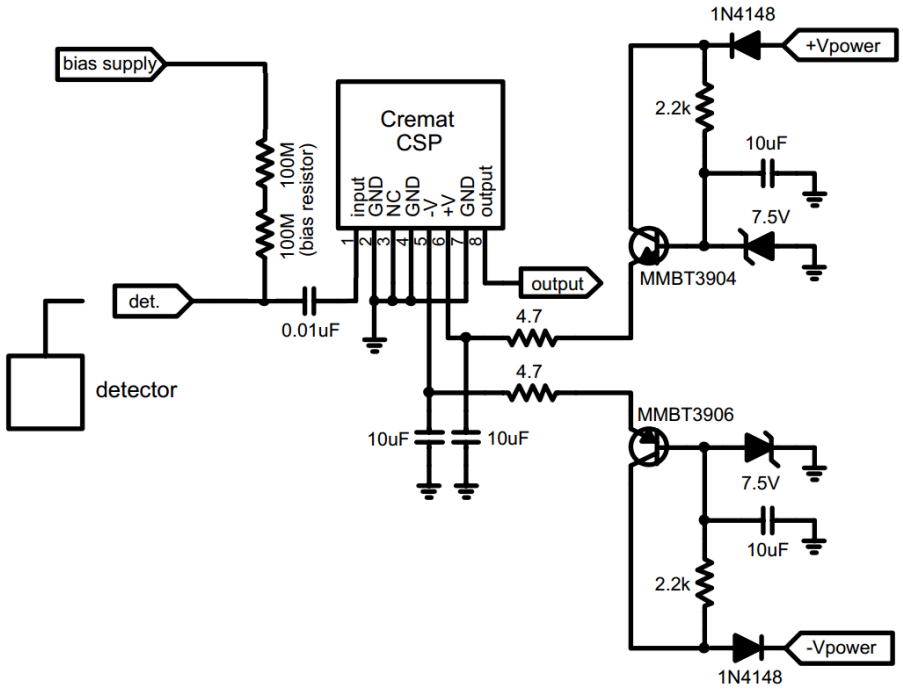


Figure 3.4: Schematic of a pre-amplifier board

## 3.4 Voltage and Current Divider

Different electrodes (induction, drift and both GEM electrodes) require different voltages to be applied to them based on the required electric field. Since only the different voltage potentials have to be applied between different plates, a simple resistor chain divider is used with one polarity. The resistors are connected in series, while each resistor reduces the voltage by the voltage drop across it. The values of the resistors are set based on the required electric field which needs to be created in any region of the detector, while the value of resistance in MΩ gives the same voltage drop value in volts when the sum of the needed voltage is applied by the high voltage source.

For simplicity, the resistance across the resistors is set to whole values based on the multiple of 50 MΩ and thus the voltage potential across the resistors is also in increments of the order of 50 V. To protect against possible current build up across GEM electrodes and possible sparks, which could destroy the sensitive GEM foil, 1000 MΩ resistors ($R_S$) are added as the figure below shows.

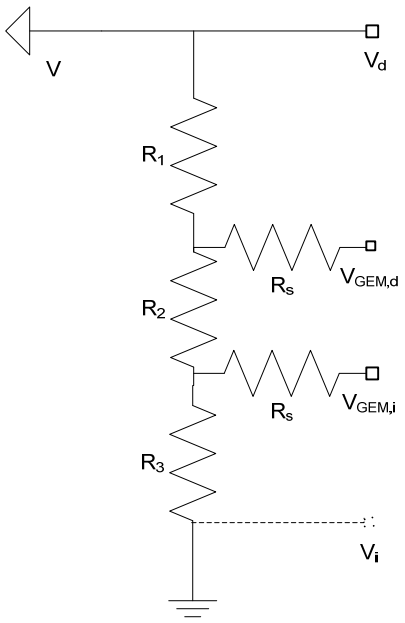


$$V_d = V$$

$$V_{GEM,d} = V\frac{R_2 + R_3}{(R_1 + R_2 + R_3)}$$

$$V_{GEM,i} = V\frac{R_3}{(R_1 + R_2 + R_3)}$$

$$V_i = 0$$

Figure 3.5: Schema of voltage divider with voltage equations

Moreover, a 20 MΩ bias resistor is placed between electrical ground (setting the voltage to 0 V) and detector bias on main board, which sets the voltage of the collection plate to 0 V. However, the resistor allows the current to flow to the pre-amplifier instead of the ground as the schema below represents. The red line represents the setting of ground voltage and blue the current flow.

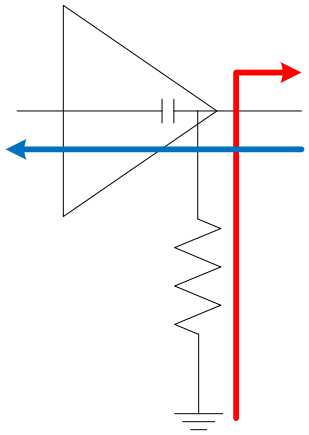

Figure 3.6: Schematic of a current divider resistor

## 3.5 Collection Plate Switch

In order to obtain an energy reading from ten individual collection plate segments by one pre-amplifier, main amplifier and multichannel analyzer, a collection plate switch is placed between the pre-amplifier and the readout stripes. Therefore the switch has ten inputs and only two outputs while the user can select any of the ten collection strips for the energy analysis. The two outputs go to either pre-amplifier or to the ground which provides ground voltage (0 V) to the unselected collection strips. By doing so, the induction field of the detector remains uniform which provides more accurate readings than having a floating voltage over the unselected read out stripes (the selected segments are set to 0 V as well by the current divider resistor that is placed before the pre-amplifier bias input).

The switch is made out of ten relays that are mounted on a custom PCB board as Shown in Figure 3.7. Due to the limited space in the existing vacuum chamber micro SPDT MOSFET solid state relays (LCC110P) have been chosen. The controller for these switches is located outside of the chamber, therefore the user can select any collection

segment without opening the vacuum chamber. Moreover, the controller provides adjusted voltage and current for the relays as they are both current and voltage sensitive.

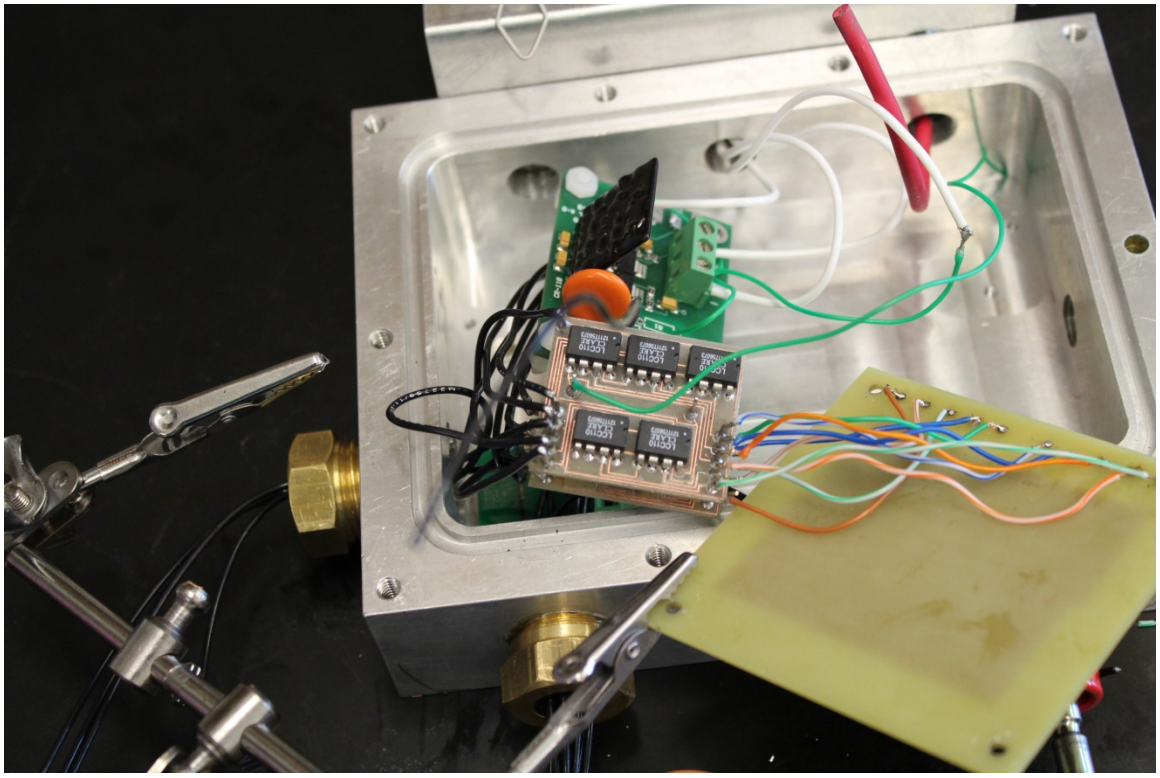

Figure 3.7: Image of connected collection plate switch

In order to reduce the noise, wires and controller are placed in an aluminum case which acts as a Faraday cage, while the controller is directly powered by the pre-amplifier voltage source. By doing so, the two systems (the pre-amplifier and controller with switch) are harmonized and the electrical noise is further reduced.

## 3.6 Selection of Gas and Pressure

The selection of the gas plays an important role as all the ionizations, scattering and multiplication process take place in gas. There are different types of gases and gas

mixtures that can be used in GEM detectors. As the main criterion for the filling gases are to provide stable gain, not to have high electron attachment and to have too low ionization energies, the most used gases are P10, $Ar/CO_2$ and $Xe/CO_2$ of which the $Ar/CO_2$ gas at two ratios 70/30 and 80/20 are the most common ones. Based on the paper written by F. Sauli [27], the inventor of the GEM, the 80/20 ratio was picked due to the GEM foil known break down point at various pressures and the higher availability of the argon over xenon gas. The break down points is located at the end of each pressure line at higher voltages shown in Figure 3.8.

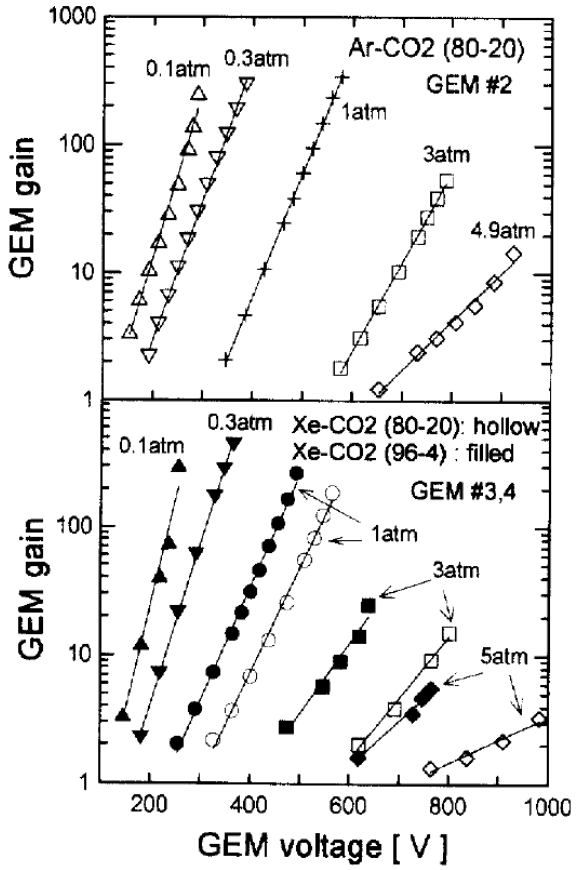


Figure 3.8: GEM gains based on different voltage potentials cross GEM at various pressures

The pressure of, $Ar/CO_2$ gas, has to be calculated based on the range of the Am-241 which emits 5.5 MeV alpha particles. As the alpha source is placed outside of the detector volume, the particle must first travel through a 2.6 mm air gap before reaching the 0.013 mm thick polyethylene terephthalate window prior to entering the gas volume. Ideally the particle should thermilize at the end of the collection plate, while most of its energy is released in the collection plate range. Therefore, the particle should still travel up to 8.4 cm in the gas, collimator and the GEM sensitive volume.

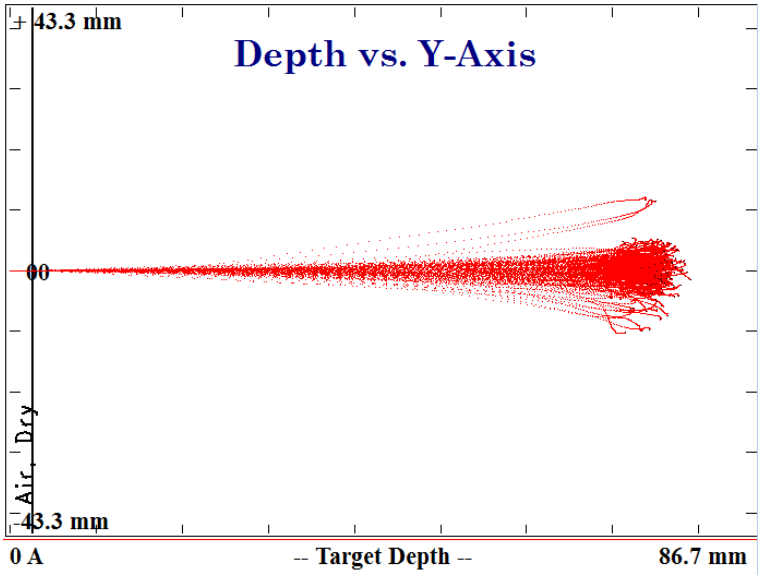


Figure 3.9: SRIM simulation of Am-241 alpha particle range for detector design

SRIM Monte Carlo software has been used to find the density of the $Ar/CO_2$ (80/20) at the given geometry and energy of alpha particle that would reach the end of the collection plate. The result is density of 0.00056 $g/cm^3$ and is used to calculate the required pressure of the gas, see Table 3.1.

| Molecule | Argon | Carbon dioxide |
|---|---|---|
| **Density at 760 torr (in g/cm$^3$)** | 0.001661 | 0.001842 |
| **Ratio** | 80 | 20 |
| **Density of mixture at 760 torr (in g/cm$^3$)** | 0.001697 | |

Table 3-1: Density of Ar and $CO_2$ gas

$$P = \frac{0.001697 \frac{g}{cm^3}}{0.00056 \frac{g}{cm^3}} \; x \; 760 \; torr \; \cong 250 \; torr$$

$$P_{Ar} = P \; x \; R_{Ar} = 250 \; x \; 80 = 200 \; torr \qquad P_{CO_2} = P \; x \; R_{CO_2} = 250 \; x \; 20 = 50 \; torr$$

The overall pressure has been calculated to be 250 torr and partial pressure of Ar and $CO_2$ to be 200 and 50 torr respectively. The gas pressure of the detector is relatively close to the value of 0.3 atm (228 torr), the pressure line from the Figure 3.8 with breaking point of the GEM foil at 380 V. Therefore, based on the scaling of the pressures, the actual voltage can be set slightly higher than the one measured by Sauli what allows an applied voltage as high as 400 V cross the GEM foil.

# 4 Chapter: Computer Simulation

## 4.1 General Principles and Settings of Simulation

The Garfield++ simulation works like any other Monte Carlo simulation and requires certain parameters like the geometry and boundary of the system, gas properties and initial particle properties to be set. As most of these settings do not change during the simulations in this chapter, they are only mentioned in this section. The changed variables for each individual simulation are provided for each simulation separately.

Moreover, the data from the simulations are only for orientation to show trends and not precise values, as the calculation times are extremely long. For this reason, only 1000 runs are averaged to create one data point in this work and therefore the error analysis of calculations is not conducted.

### 4.1.1 Geometry and Boundary Conditions

The geometry simulation settings are exactly the same as the physical settings discussed in Chapter 2 where the drift region is 9.1 mm wide and induction region 1.3 mm. The standard GEM foil dimensions are used with 50 µm thick kapton and 5 µm thick copper electrodes. The copper rim (hole through electrodes) has diameter of 70 µm and the outer and inner diameter of the bi-conical hole though kapton are set to 70 µm and 50 µm respectively. The boundary conditions of the simulation are set to contain the whole height of the sensitive volume with 1.5 by 1.5 mm cross section. This

cross section is sufficiently big enough to accommodate the electron diffusion at low electric fields.

### 4.1.2 Gas Settings

Similarly to the previous section the gas setting of gas properties is obtained from Chapter 2. The gas is defined as argon and carbon dioxide with ratio 80/20 with room temperature 293.15 K at 250 Torr. Since the program cannot calculate and does not have a database for the penning transfer of the mixture, it is set manually to 0.51. This value is determined by gain curve fits as describe by Sahin [28]. Similarly, mobility of negative ions ($O^-$), created by electron attachment, must be imported manually. For this reason, data of ($O^-$) in $CO_2$ was obtained from Transport Properties of Gaseous Ions over a Wide Energy Range paper [29] and are presented in Appendix B.

### 4.1.3 Initial Particle Setting

Due to the inability of alpha particle tracking in Garfield++, the simulations are done by placing electrons that would be created from the alpha particle ionization into the drift region. The electron is set to have a 0.1 eV energy with randomized initial location as the alpha particle can move anywhere within the trajectory of the beam while the initial direction of the electron is also randomized.

## 4.2 Drift Field Simulation

The drift field in the GEM detector must be carefully chosen in order to ensure stable gain of the whole system since the ionization of the $Ar/CO_2$ gas by the initial alpha particle take place in this region. Even small irregularities in electron production from

ionization and their subsequent transfer to the GEM will cause large irregularities of the overall detector signal as electrons will get multiplied. Therefore, the drift field must be set in the ion chamber region where the potential difference between the GEM foil and the drift electrode is strong enough to overcome recombination of the ion pair right after the ionization, but not to cause further ionization by the electrons (secondary ionisation).

For this reason, an ion chamber experiment was set up so to take place between the drift electrode and the GEM drift copper electrode. The voltage potential between the electrodes was varied as the pressure was set to the same operational pressure of the GEM detector (250 Torr) and $Ar/CO_2$ concentration (80/20).

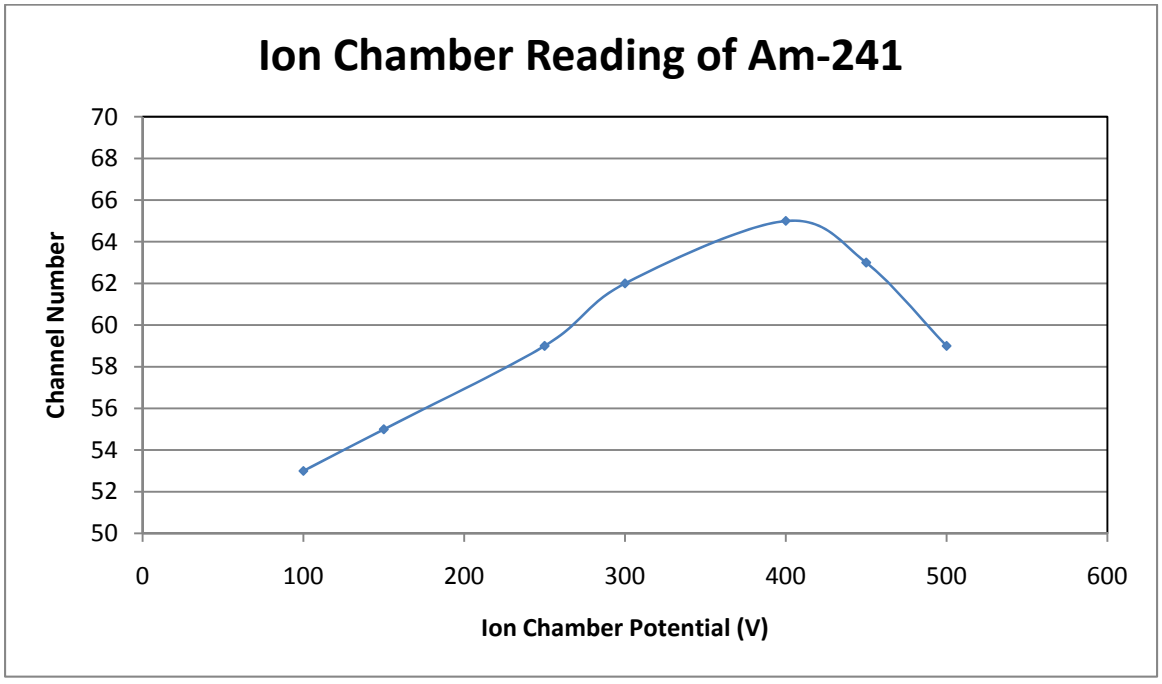


Figure 4.1: Experimental ion chamber readings at different voltage potentials

The figure above shows that the energy reading from the detector initially increases with the increasing voltage difference as less ion recombination takes place at

higher voltages. However, after around 400 V the detector reads lower energies for the same 5.5 MeV alpha particle. This is due to the higher electron absorption of the $CO_2$ gas, as more electrons reach higher energies laying within 3.1 - 10.05 eV $CO_2$ electron attachment regions as the figure below suggests.

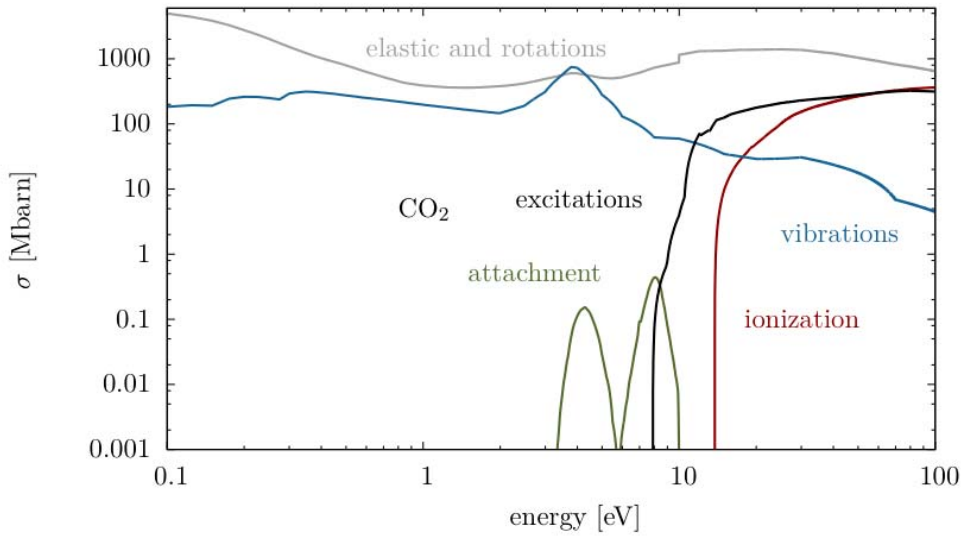


Figure 4.2: Electron cross sections of carbon dioxide gas

Garfield simulation of the ion chamber region shows a consistent result with the discussion above where more electron attachments occur at higher drift potentials. As a full simulation of the initial ionization is not possible in Garfield, the simulation of ion electron recombination is also not possible. Electron attachment at different drift fields is presented in Figure 4.2 with two different electron drift distances of 4.5 and 9 mm (distance from initial ionization to the collection plate). The electron attachment fraction stands for how many electrons have been attached to the gas molecules when compared to the initial number of placed electrons to the gas mixture. Moreover at high electric fields some of the electrons undergo to further ionization of the gas and create

additional electrons. For this reason, the electron attachment fraction can be above 1 as there are more electrons (that could be attached) created by secondary ionizations when compared to the originally placed electrons.

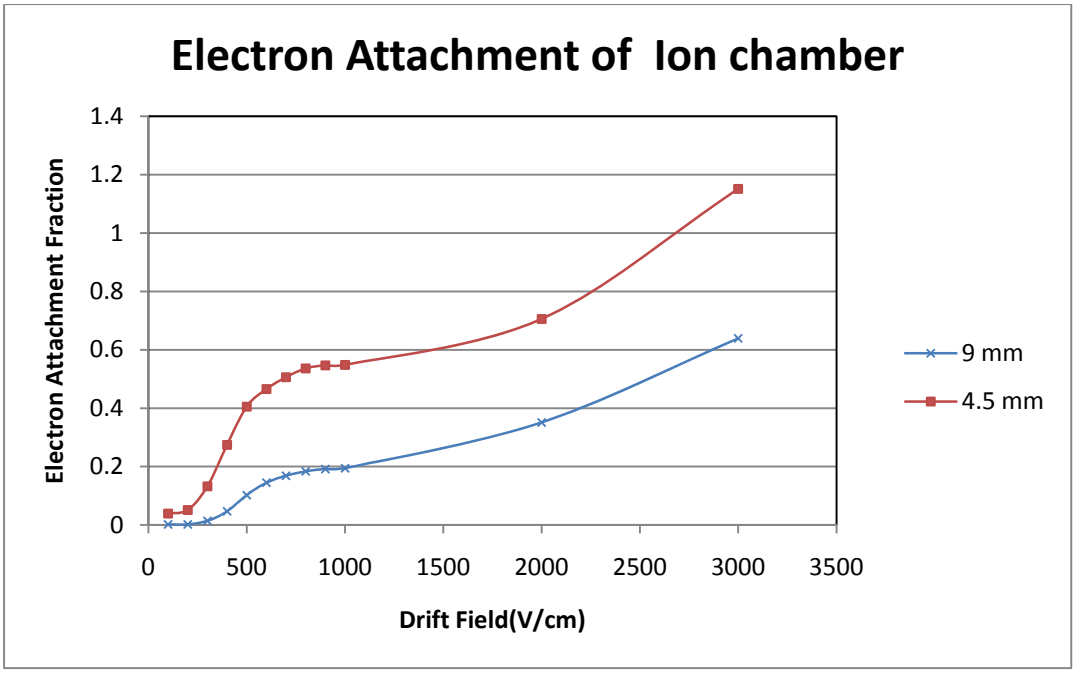


**Figure 4.3: Garfield simulation of electron attachment between two parallel plates of an ion chamber at different electric strengths**

A second important feature of the drift field is to transfer the electrons towards and through the GEM foil. In general, the electrons follow the field lines when not considering transversal diffusion and scattering of the electrons. The shape of the field lines is strongly linked to the voltage potential difference between the drift electrode and GEM foil due to the small GEM channels. As the voltage difference in the drift region increases, the field lines curve less towards the GEM channels and tend to curve inwards at lower voltages as shown is Figure 4.4. The drift voltage difference is set to 300 V on left and 600 V on right.

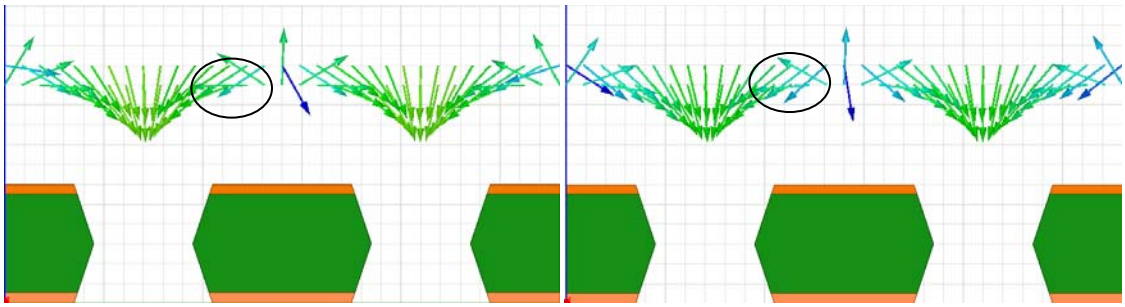

Figure 4.4: Electric field vectors representing different curvature of field lines in drift region.

Consequently, the GEM is less transparent to the electrons as they do not drift towards the holes, but to the copper foil, at higher voltages. The electrons collected on the copper foil no longer contribute to electron avalanches, and this weakens the detector output signal. Garfield simulations show consistent results with the proposed theory in Figure 4.5. Moreover, the graphs shows important feature of the electric field on the transparency of the GEM foil, the dependence on location of the initial ionization (electron creation point). The further away from the GEM foil the ionization takes place, the better the GEM foil's transparency appears at high drift potentials.

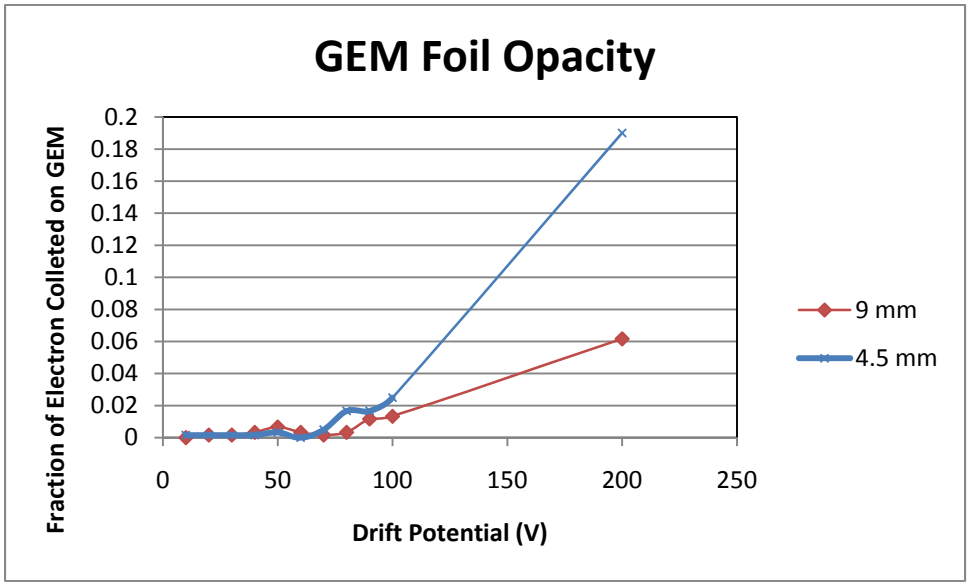


Figure 4.5: Garfield electron transparency simulation

## 4.3 GEM Field Simulation

The GEM can be considered as an analog signal multiplier where electrons coming from an ion chamber, the drift field, are multiplied before they are collected in induction region. The strength of electric field between the GEM copper foils is only dependent on the voltage difference between the two foils as the distance is fixed. Therefore, the electron multiplication directly depends on the applied voltages a cross this section as well as on the type of gas and its pressure. The electron avalanche size as a function of the applied voltage potential cross the GEM is presented in figure below, where all the electrons are comprised of the part of the avalanche which passes though the foil, together with electrons that land on the kapton and copper foils. GEM potentials higher than 400 V are not applicable due to the physical limitations of the foil for a given gas type and its pressure.

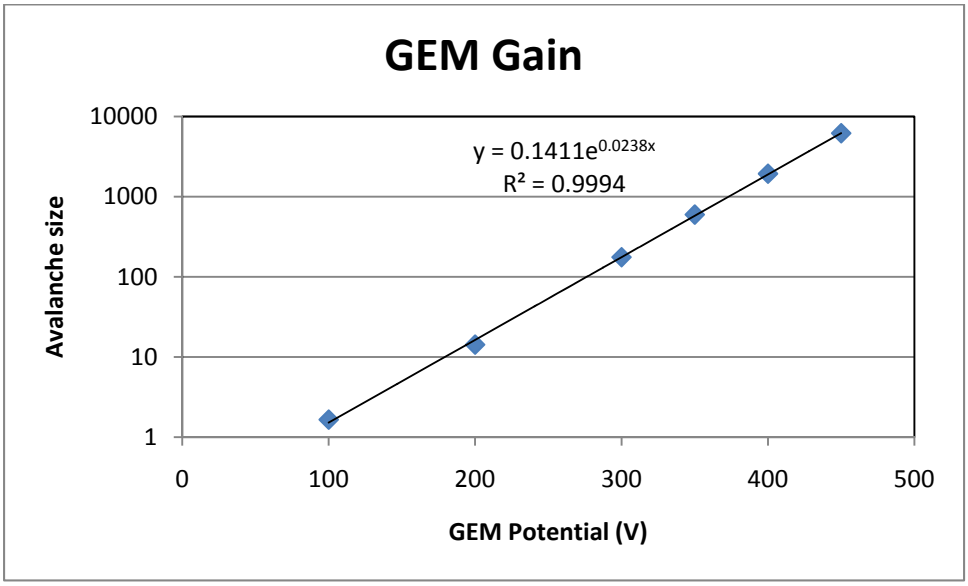


Figure 4.6: Garfield electron gain simulation across GEM at 250 Torr and $Ar/CO_2$ (80/20) gas

The high gain of the detector is possible due to high electric field that is produced between the GEM electrodes. The Maxwell software shows that the electric field in middle of the GEM can reach almost 100 kV/cm at potential 400 V. Moreover, the model shows that any electron relatively close to the GEM induction electrode would get collected by it as the eclectic field vectors are directly pointing to GEM.

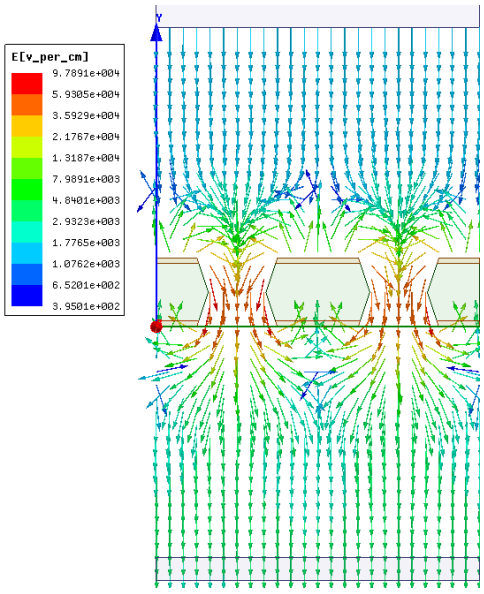


Figure 4.7: Electric field simulation of the GEM detector with electric field vectors

## 4.4 Induction Field Simulation

The purpose of the induction field is to transport the electrons to the collection plate (induction electrode). Similar to that in the drift field, the shape of the field lines and the electron attachment directly depend on the strength of the electric field in the induction region. Moreover, at high electron gains, electrons diffuse closer to the induction GEM copper foil and can be collected by it. The field lines in this case should be as much extending to the collection plate as much as possible so that electrons would not follow along the field line to the GEM induction copper foil. This is achieved

by applying a high potential difference between the GEM and the induction electrode and creating a strong electric field. Figure 4.8 shows how the direction of the field lines changes with increased induction fields. The induction voltage difference is set to 500 (top left), 2000 (top right) , 3000 (bottom left), 9000 V (bottom right).

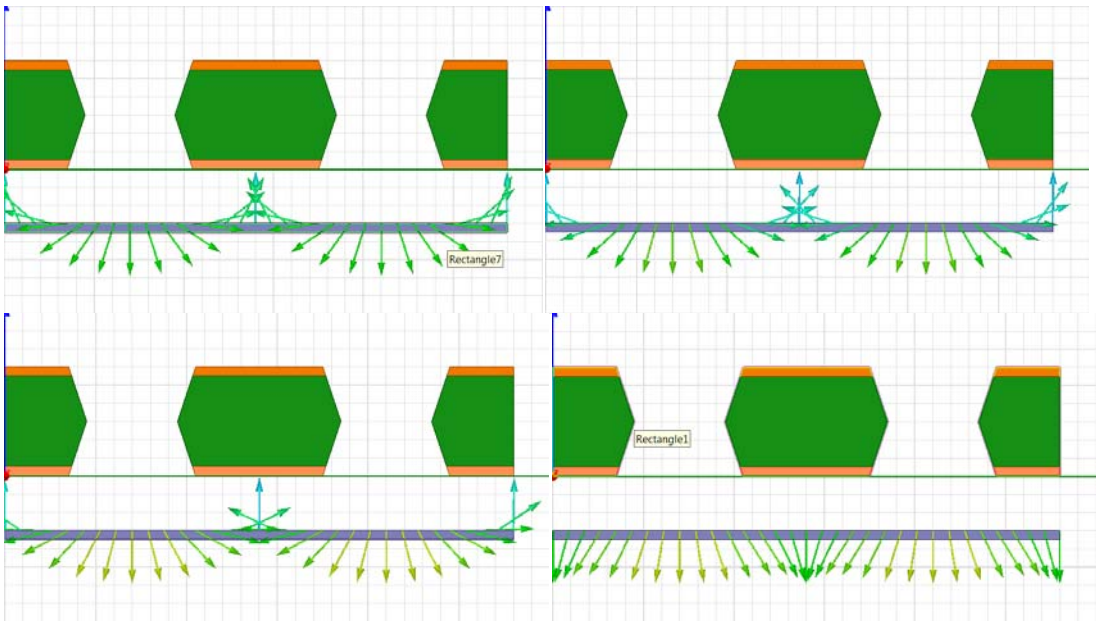


Figure 4.8: Electric field vectors representing different curvature of field lines

As the induction field is significantly weaker than the GEM field, it does not influence the size of avalanche within the GEM. However more electrons, which are created within the GEM region, reach the collection plate at higher induction potentials due to the field line change of direction as Figure 4.9 shows. These values already consider the increase probability of electron attachment at higher induction fields.

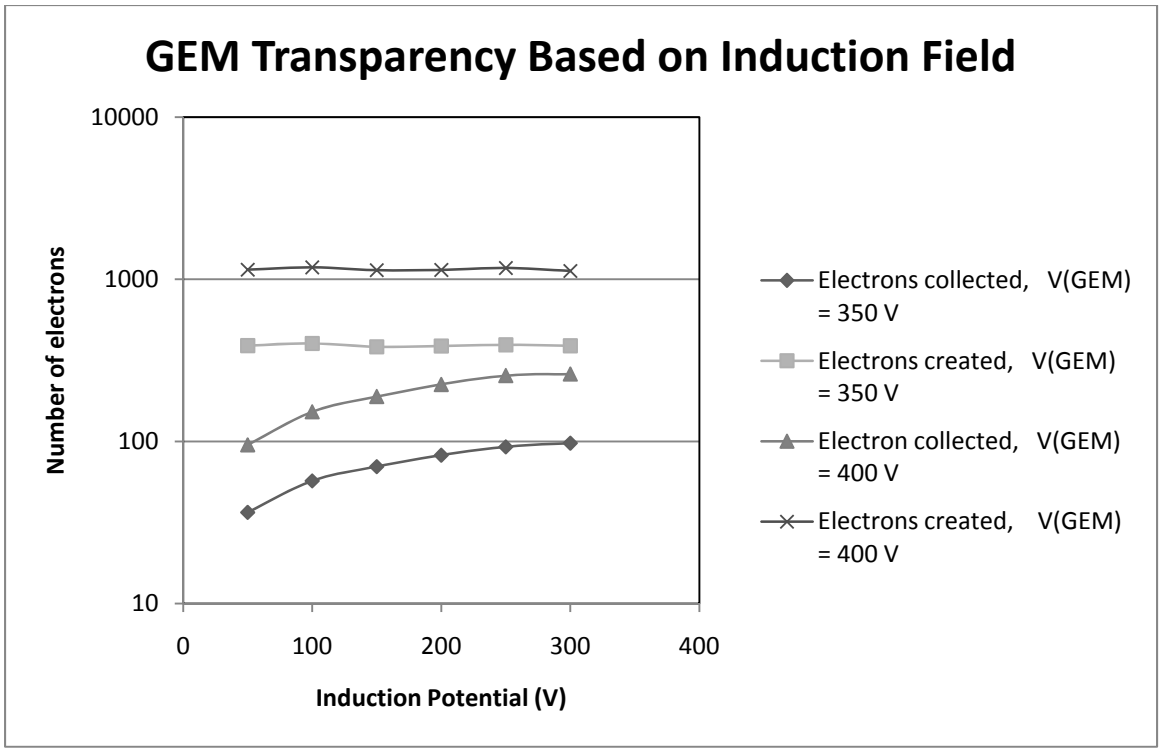


Figure 4.9: Garfield simulation of GEM foil transparency based on the induction field strength

The electrons leaving the GEM foil have various energies as electron energy varies based on the field that the electrons drift through, the distance from its previous ionization and the energy that they lost during the ionization process. The upper limit of the electron energies, leaving the GEM at a distance of 20 µm, is around 30 to 35 eV. As this value is relatively high and part of the strong GEM field reaches to induction field area there is a significant additional multiplication happening within this region. In case of a GEM with potential 350 V the ratio of induction electrons to GEM electron slightly increases with induction field strength from 36:64 to 40:60 as Figure 4.10 represents. Similarly for GEM with 400 V voltage drop the ratio changes from 43:57 to 47:53. This is mainly due to higher electron energies obtained in the stronger induction fields which allow them to do further ionizations and contribute to the overall electron production.

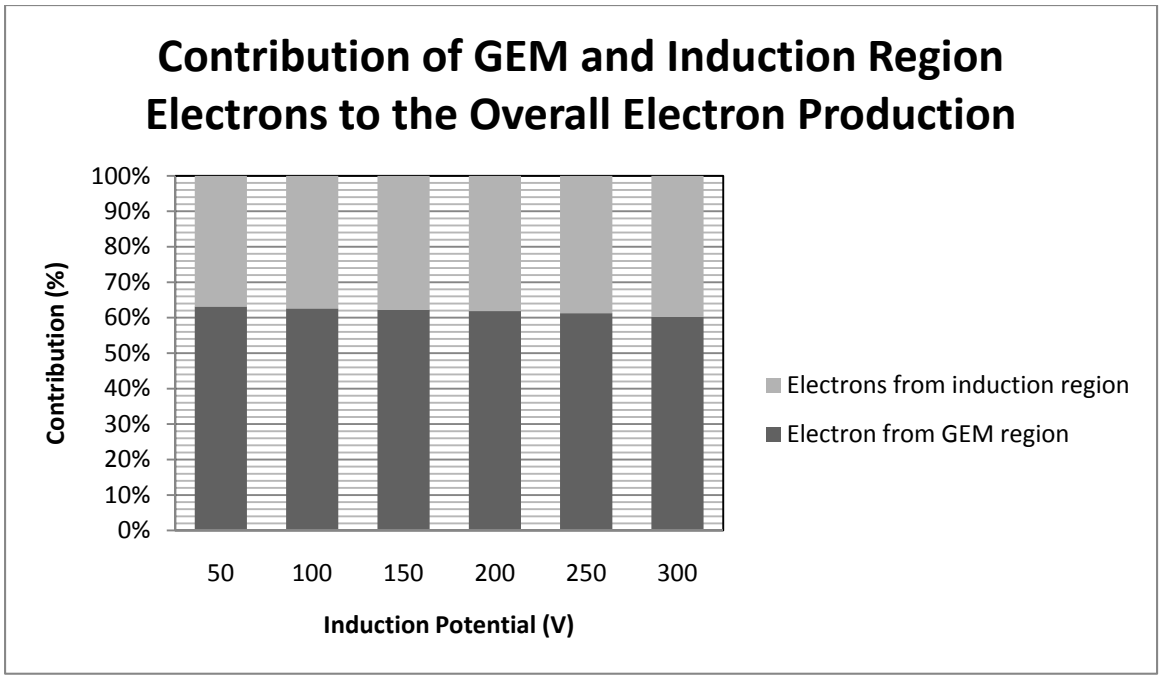


**Figure 4.10: Garfield simulation of electrons contribution from GEM (350 V) and induction region to the overall avalanche**

When considering only the electrons that are used for signal build up (the electrons that reach the collection electrode) the distribution of 1:1 ratio is found at lower induction values and increases slightly to 3:4 (GEM electrons to Induction electron). This can be seen on a figure bellow, which shows the composition of the electron that contributes to overall number of electrons collected. The figures also represent the overall useful gain of the GEM detector with GEM potential of 350 V and 400 V at various induction potentials.

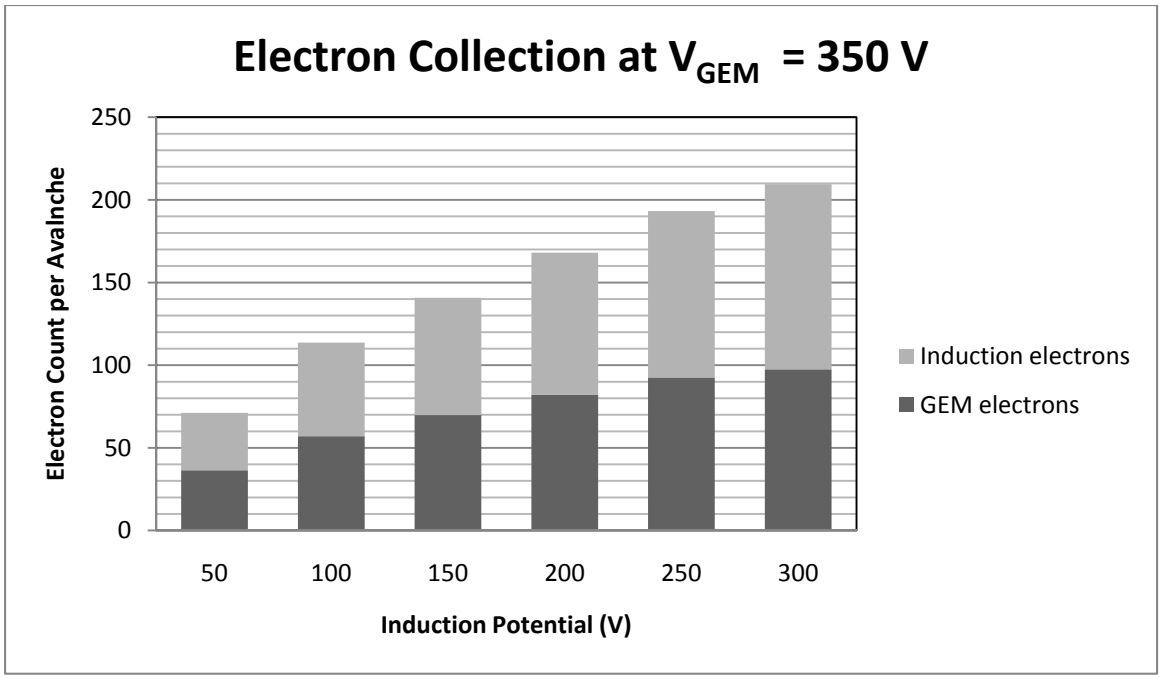


Figure 4.11: Garfield simulation of electron collection with GEM potential set to 350 V

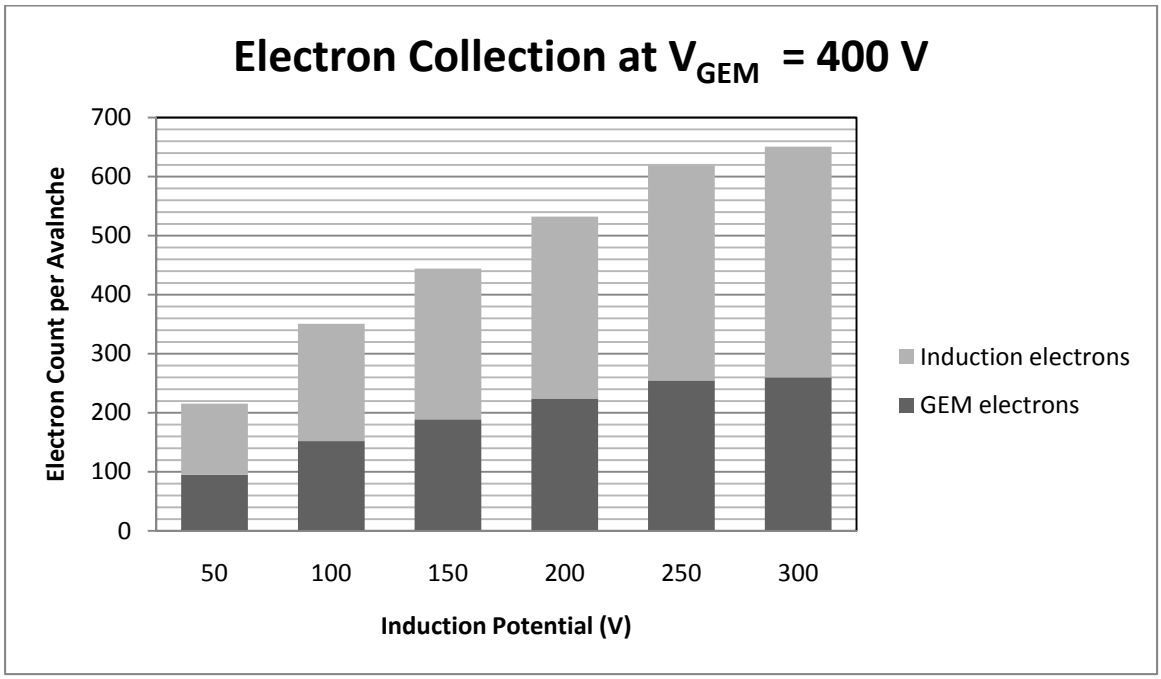


Figure 4.12: Garfield simulation of electron collection with GEM potential set to 400 V

On the other hand, these high values of additional multiplication over a larger distance (the thickness of induction field), when compared to the thickness of the GEM

foil, leads to less stable gains and therefore broader measured energy distributions at higher induction fields. When applying higher potential drops across the GEM foil the higher gains produce more electrons which have sufficiently high energies leaving the GEM to produce further ionizations even in the induction field. Moreover, Figure 4.13 shows that the gain fluctuation increases at higher gains which means longer measurement times in order to get the same statistics.

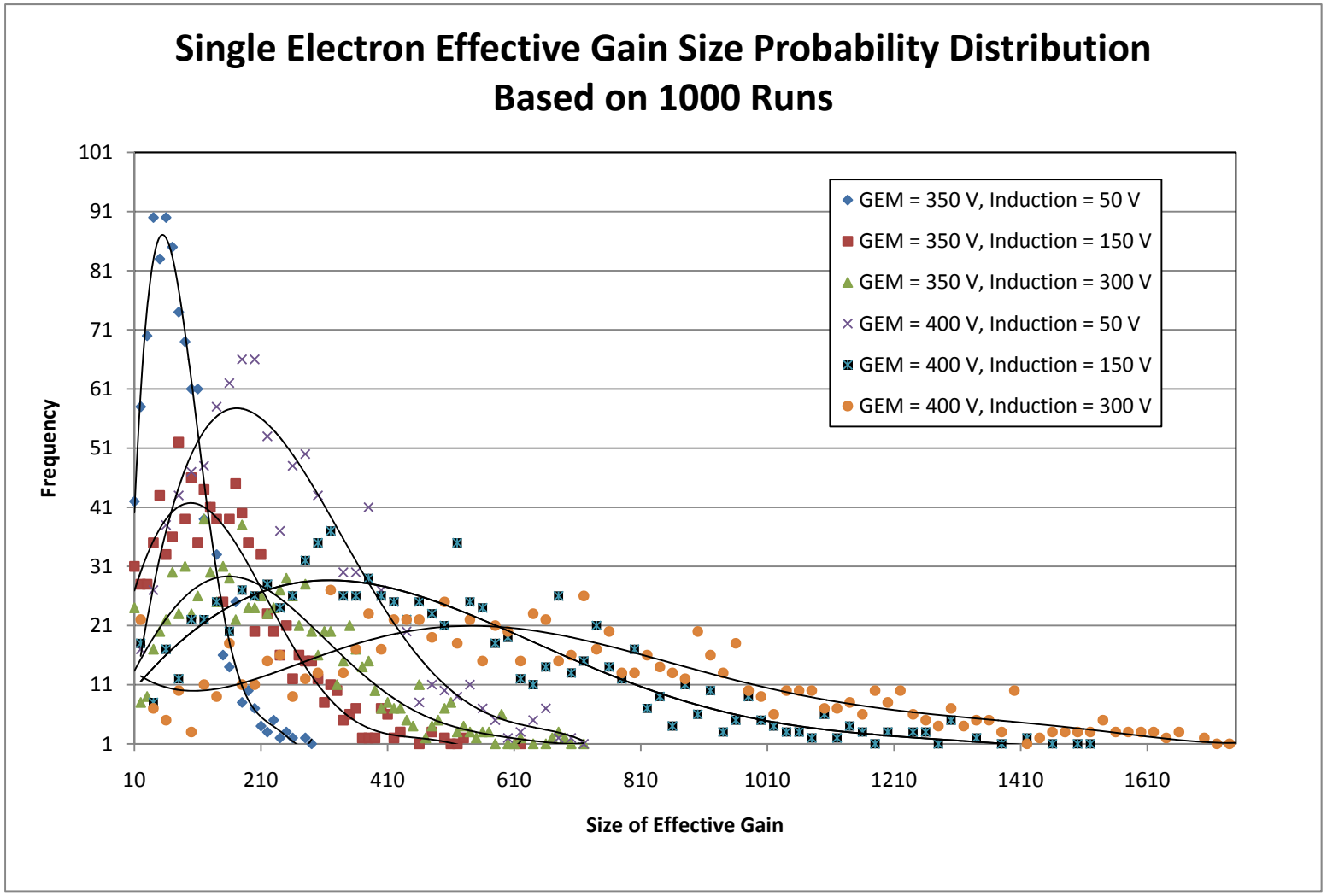


Figure 4.13: Garfield simulation of distribution of collected electrons

Moreover, the higher induction fields increase the average energy of the drifting electrons closer to the electron attachment energy range of the gas, which leads to a high number of electrons that escape the useful detector gain. These electrons get attached primarily to the $CO_2$ molecules, as its electron attachment cross section is significantly higher than that of Ar and they create an unstable $CO_2^{-}$* ion (the $CO_2$ molecule has much higher electron affinity than Ar due to the oxygen fragment) [30]. The $CO_2^{-}$* further dissociates into a stable C0 and $O^{-}$ molecule. In overall charge contribution to the collection plate the negative ions $O^{-}$ can contribute to it by up to 13 % in both cases with the GEM potential set to 350 and 400 V. The results are shown in figure bellow while the data are identical for both cases of GEM potential. This could possibility lead to detector noise at high particle rates.

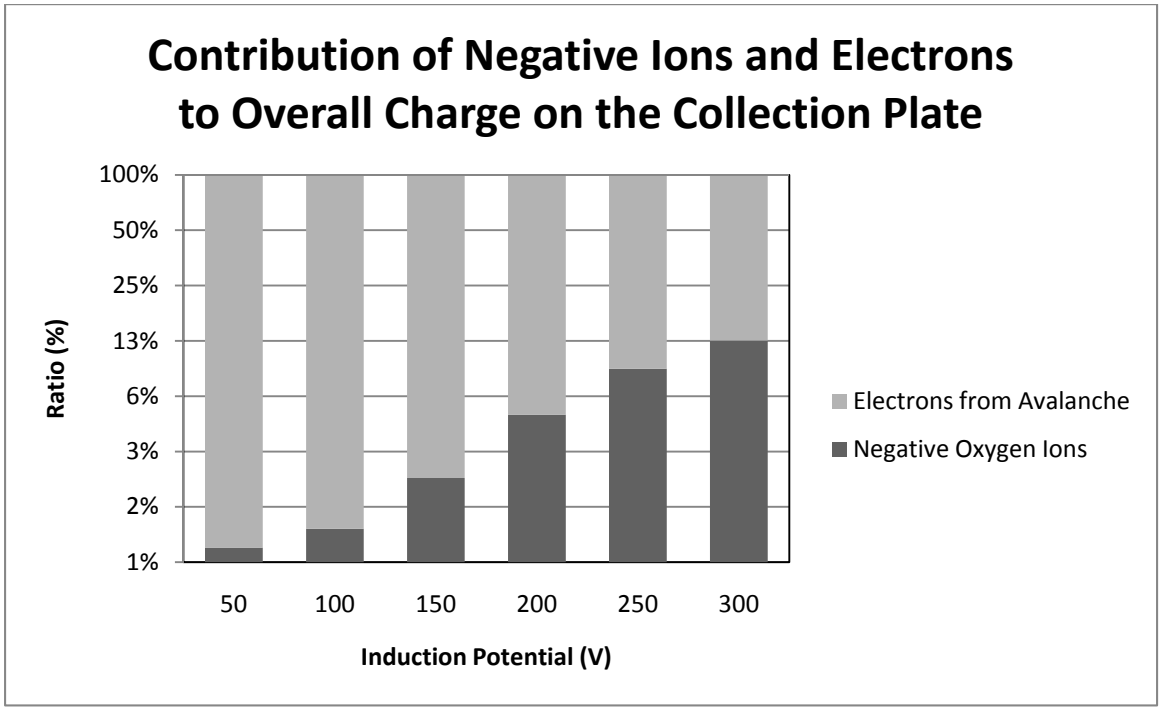


**Figure 4.14: Garfield simulation of collection plate charge distribution based on number of electrons and negative ion**

As the negative ions $O^-$ drift significantly slower to the collection plate than electrons from the avalanche, they arrive at the collection plate considerably later than the electrons. However, the collection time distribution for negative ions is much greater than the one for electrons. The figure below (Figure 4.15) shows different collection times for negative ions from a single avalanche and their standard distribution with manually inputted ion mobility of $O^-$ in $CO_2$ gas (see Appendix B). Moreover, the autodetachment of the extra electron from $O^-$ molecule is not possible since the induction field is well below 22.5 kV/cm (given by 90 V/cm Torr) [32].

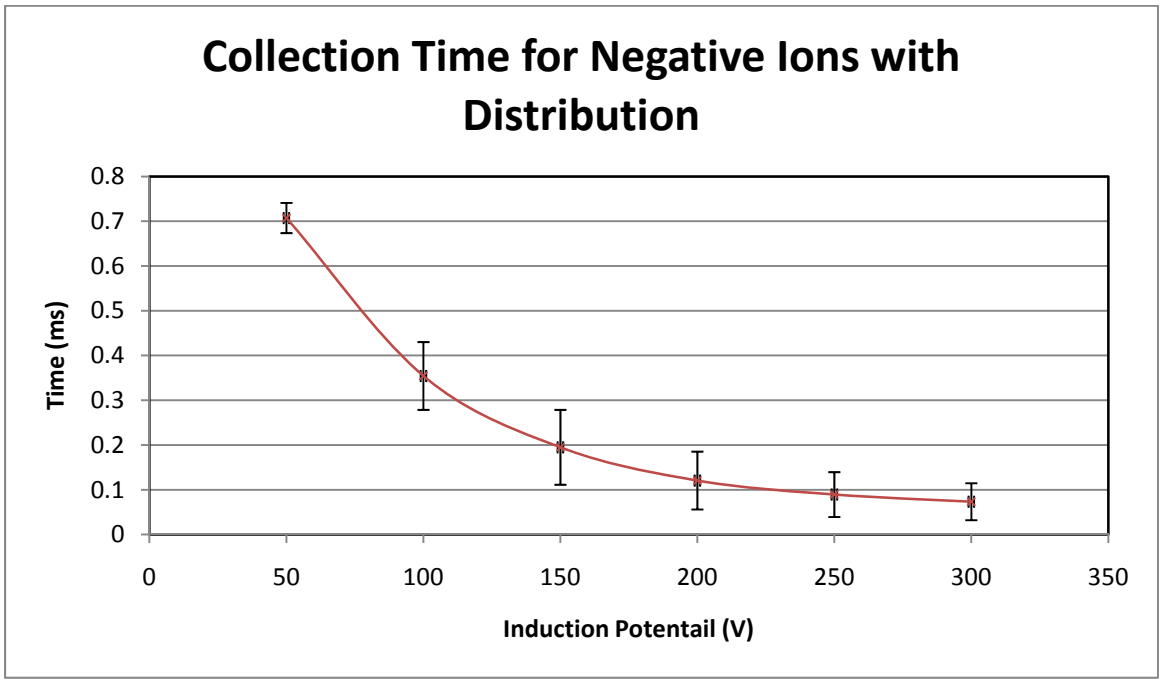


**Figure 4.15: Garfield simulation of collection time for negative Ions with distribution for GEM potential 350 and 400 V**

In the case of electron collection, the mean collection time is much shorter around 110 ns with standard deviation of around 50 ns. For this reason, the negative ions might not create any noise or very low level noise, even with shorter collection times and

smaller standard deviation as seen at the higher induction fields. However, the negative ions might cause significant noise at high count rates.

## 4.5 Summary of Computer Simulation

The simulations of various conditions has been carried out by the use of the Garfield++ tool kit in order to save time and mainly to avoid possible equipment destruction (such as damaging the sensitive GEM foil). Based on the data obtained from the previous part of this chapter, the general characterization of the system can be made.

The drift region needs the lowest electric field possible as the electron absorption and GEM transparency increase at high electric field. However, the field must be strong enough to overcome recombination of the ion and electrons created from the initial alpha particle ionization. By considering both requirements, the drift region is set to 450 V a cross the electrodes.

The GEM foil should be set to the highest value possible but below the value at which avalanche becomes unstable or sparking through GEM foil occurs. In our detector configuration, the limiting value of volatege on GEM foil is 350 V but, it could possibly be as high as 400 V because our experimental conditions are different from those that Dr. Sauli (referring to Figure 10 in Chapter 2). Since the computer simulation can not simulate sparking or stability of avalanche, both of the above mentioned voltage values need to be tested.

A similar situation emerges in defining the induction field where higher voltages provide additional gain, but on the other hand increase electron attachment. This does not only decrease the size of the avalanche and creates broader peaks but could be a possible source of noise from the created negative ions. For this reason, high and low induction fields should be tested as the computer simulation can not predict the sensitivity of the pre-amplifier to the slow negative ions.

# 5 Results of Detector Prototype Tests

## 5.1 Prototype Overview

A GEM energy tracking detector has been constructed based on the parts describe in Chapter 3. However, during the preliminary testing of the device, sparking occurred a cross the GEM copper electrodes and partially destroyed the GEM foil. Unfortunately, due to extremely long waiting periods for new framed GEM foil, the current prototype operates with a GEM that can only support 200 V at the designed detector condition (pressure). This value is significantly lower than the detector design criteria which assumed to use 350 and possibly try 400 V and leads to a decrease of detector gain to around 10 instead of 250 ($V_{GEM}$= 350 V) or possibly 650 ($V_{GEM}$= 400 V). For this reason, the detector has been set to a higher induction field, as this can provide additional gain when compared to a lower induction field. The possibility of creating large quantities of negative ions is suppressed by the low gain. The set up of the detector resistor board with voltage drops across the various regions with its input high voltage is presented in the table below.

| Field | Voltage drop (V) | Resistor (MΩ) | HVS (V) |
|---|---|---|---|
| **Drift** | 450 | 450 | 950 |
| **GEM** | 200 | 200 | |
| **Induction** | 300 | 300 | |

Table 5-1: Settings of the prototype detector

Even though the detector suffers from the low gain some measurements were still possible due to the very low levels of detector noise (around 7 mV) which have been achieved by precise wiring of the detector and the use of a high sensitivity pre-amplifier.

An example of pulse shape from the detector before being amplified by the main amplifier is presented below with the detector noise.

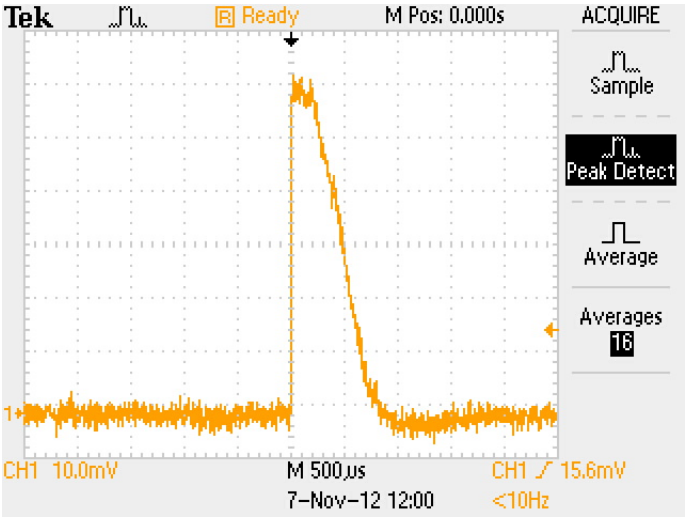


5.1: Example of pulse from the GEM detector

Furthermore, the collimator has been slightly modified during the testing due to charge build up on the Teflon tube over the time (approximately 3 hours at 450 V drift potential)), which was producing negative voltage peaks instead of stable voltage output. The problem was fixed by a reduction of the outer diameter of the collimator while the inner diameter remained the same.

However, this mechanical collimation is still not ideal mainly due to extremely low count rates, around 1 count every 10 second with the available Am-241 source with an activity of 3.867 kBq (January 2011) . For this reason, any kind of measurement with this detector and source takes a significant amount of time in order to get reasonable statistics.

Overall, besides the change of detector gain the rest of the detector is identical to the proposed and explained design. The inside of the detector prototype with its electronics is presented below. The stack of drift, GEM and collection plate is located under the resistor chain board. The collection plate switches consist of two boards that are stack on top of each other, while each of them has 5 relays (on the figure they look like small computer chips). The pre-amplifier board with the pre-amplifier chip are occupying the rest of the space of the aluminum chamber.

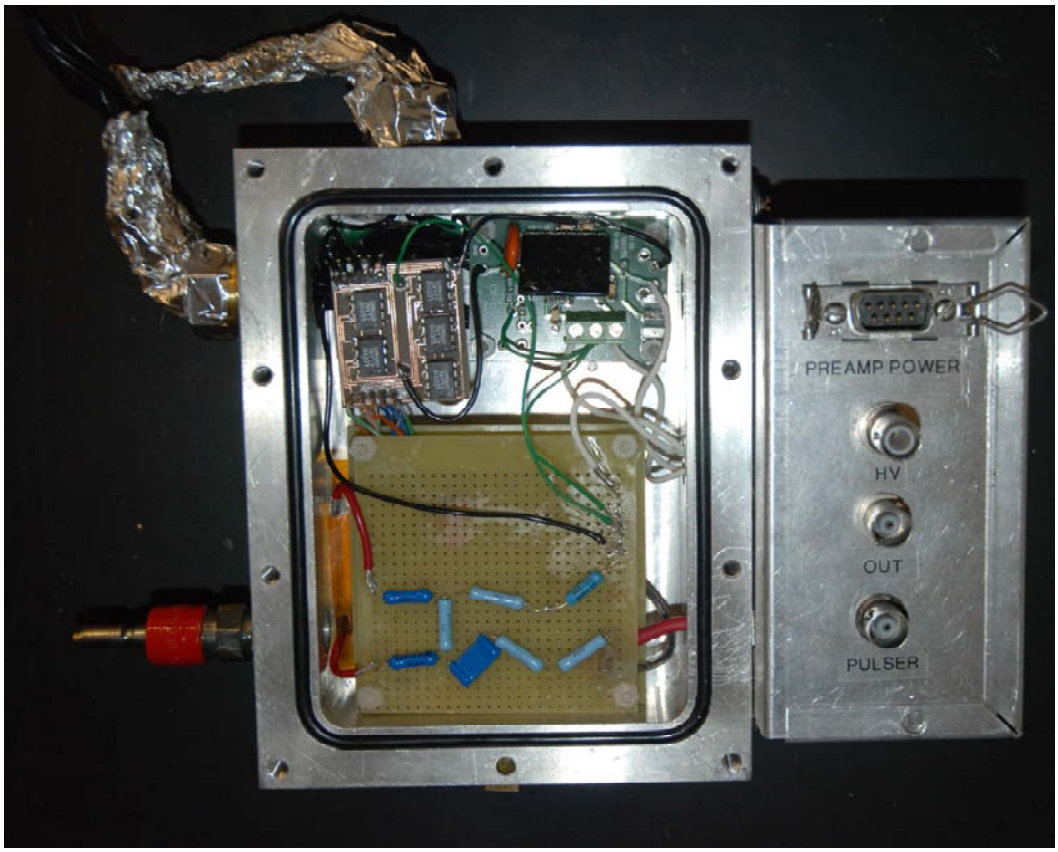


Figure 5.2: Image of the internal parts of the physical detector

During the experimental measurements the detector is fixed by two G-clamps which provide stability to a detector due to is feed though at the bottom and right side

and straight horizontal surface for the Am-241 source which is freely placed on top of the detector entrance window. The Figure 5.3 shows the standard setup of the system with connected oscilloscope which provides visual understanding of the detector status and is used for problem detection like noise, charge build up or possible sparks.

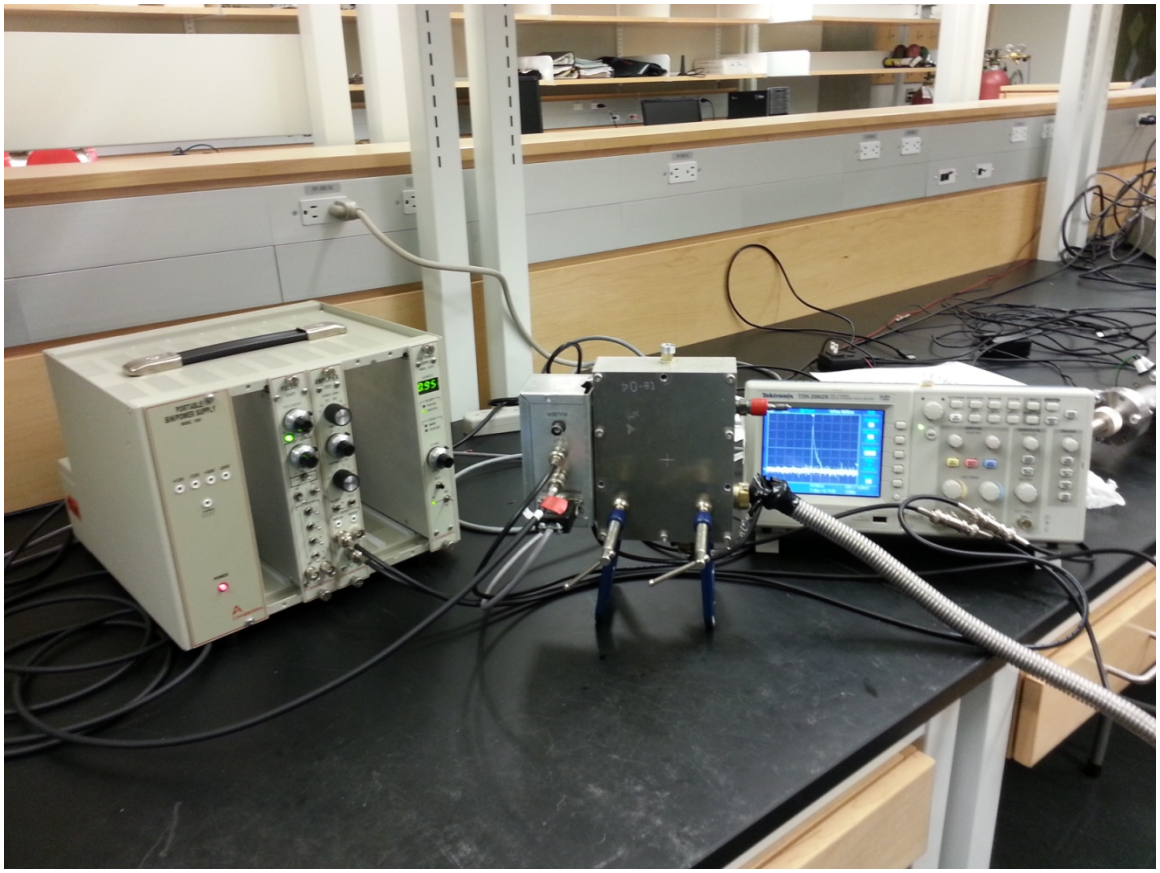

Figure 5.3: Image of general setup of an experiment

## 5.2 Energy Tracking of an Alpha Particle

As the main goal of this work is to obtain measurements of alpha particle stopping power, an experiment with this prototype have been conducted. However, due to the detector lack of gain some data could not be measured as the pulse height did not exceed the detector noise. However, the main problem during the measurement was

the additional break of one micro relay, which controlled the collection plate number 7 (the number of collection plate increases with distance traveled from the collimator), where the possible Bragg peak should be located. The data of the experimental work are shown below, while collection plate number 9 and 10 show very small energies and could not overcome the lower level discriminator which was set to 28 channels. For this reason, they have assigned 0 values as undetectable.

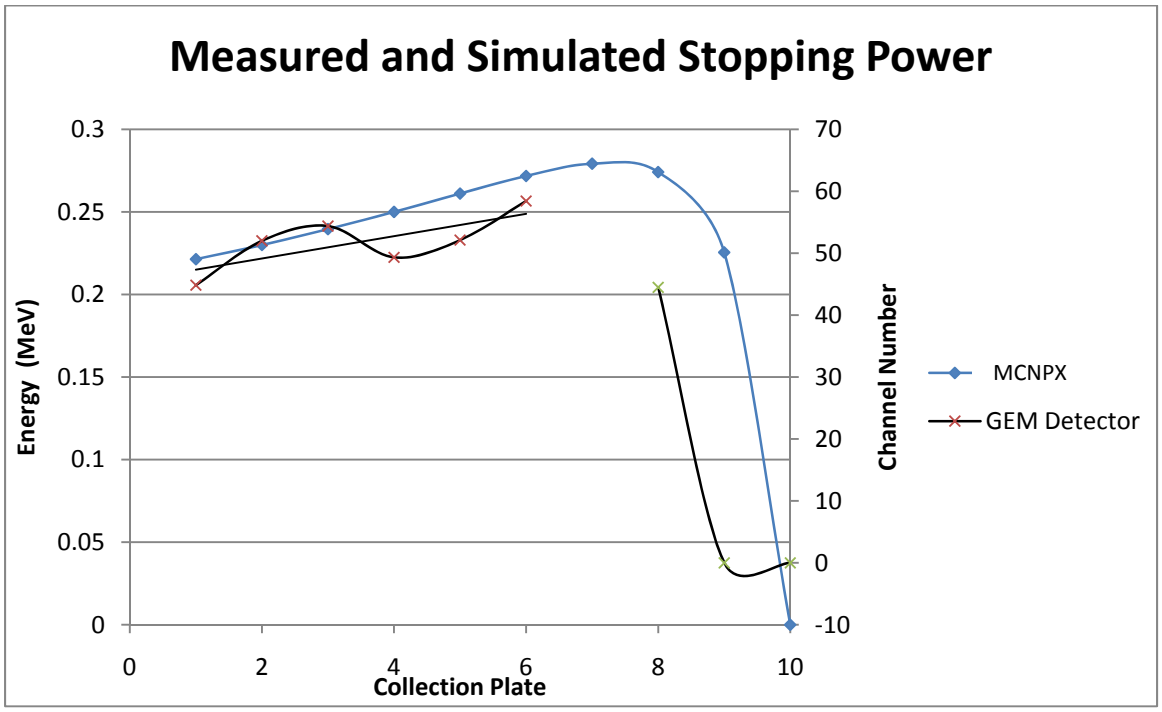


Figure 5.4: Measured and simulated stopping power of an alpha particle

When comparing the data to a MCNPX simulation (the left axis applies) , one can see that the theoretical experimental Bragg peak is shifted which could be due to possible deposits (just couple micrometers) on the entrance window. Moreover, the data from number 2 and 3 collection plates do not match the general trend of the stopping power curve. The possible reasons behind this offset could be the partially

destroyed GEM or small scratch on the collection plate. Unfortunately, data for collection plate number 7 are not possible, due to the unexpected breakdown of its switch. However, based on the general trend of the measured stopping power, initially the energy slightly increasing with alpha particle travelled distance and by the end sharply decreases, one could expect the Bragg peak to be located in this region.

## Stability of the Detector Pulse Height

In order to ensure the stable performance of the detector 2 measurement have been taken over a time period of 72 hours from the initial gas fill up, one at the beginning and one at the end of the energy tracking experiment. Each time the detector was set to perform long tests to provide reasonable statistics of the measurements. Prior to these experiments the detector has been degassed for 3 days and refilled two times.

The detector was set up to collect energy reading from the whole collection plate, the segmentation was turned off by the collection plate switch, in order to get highest peak possible. Moreover, 300 V voltage drop have been selected for the induction region as it provides highest gain based on the computer simulation since the gain of the GEM foil is already reduced.

The table below shows the data obtained from the 2 readings with times of the experiment, overall number of counts, energy peak reading and the resolution of the given reading.

| | Time form Gas Filling (days) | Number of counts | Peak channel reading | FWHM |
|---|---|---|---|---|
| **Test I** | 0 | 471 | 154 | 10 |
| **Test II** | 3 | 482 | 155 | 15 |

Table 5-2: Detector stability statistics

The detector shows very small drift over the 3 days, only by one channel which can be considered negligible. An example of one of this data set is in Figure 5.5. The long left shoulder statistics on the left side of peak in mainly due to the scattering of alpha particle in the collimator and from the source itself.

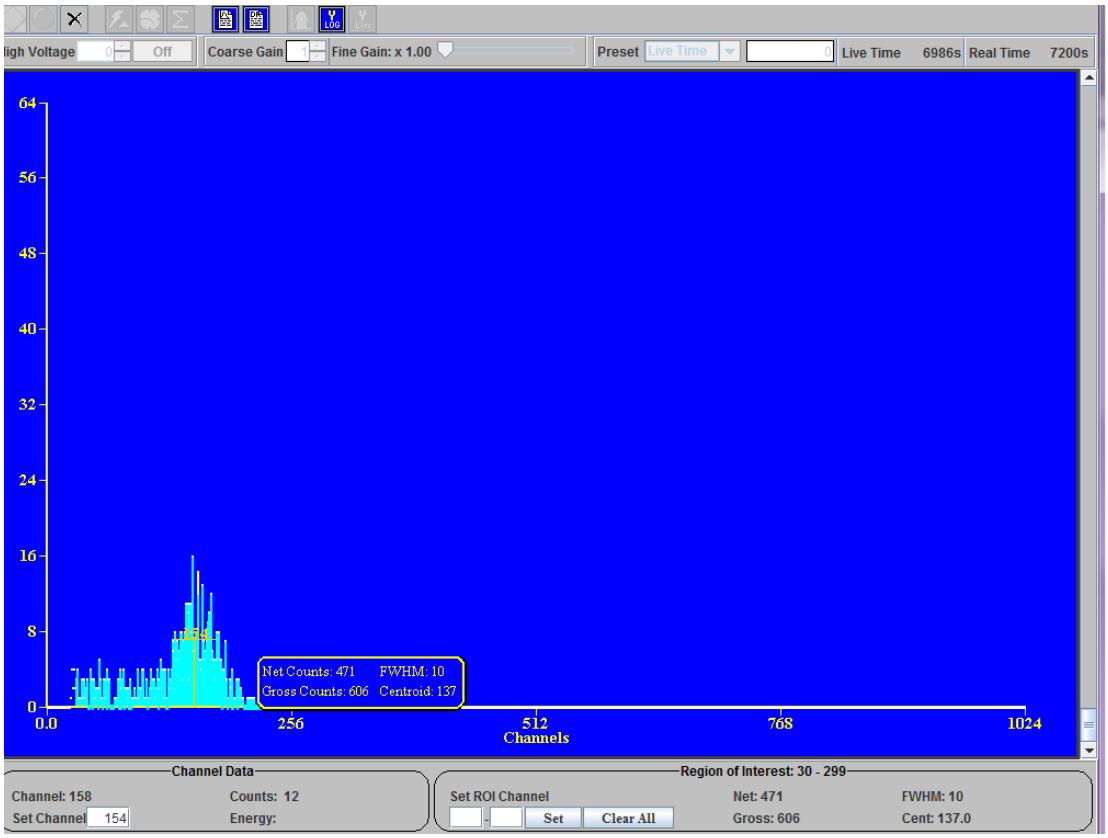


Figure 5.5: Example of peak obtained during the stability measurements

# 6 Chapter: Conclusion and Future Developments

The main objective of this work was achieved by simulation, design and construction of a GEM detector for particle tracking using an Am-241 source. This study was also aimed at improving an understanding of the working principles of GEM detectors, mainly the transport of electron from primary ionization to the collection region and to give a general guidance for the construction of similar kinds of detector.

The Monte Carlo and field simulation studies provided a strong understanding of the GEM detector general design while it also helped to understand particular behaviours of the detector.

The final prototype was unfortunately not completely capable of fulfilling the task of measurement of the alpha particle track by stopping working mainly due to a malfunction of one collection plate relay. Moreover, the detector was not capable of achieving simulated and designed gains due to the breakdown of the sensitive GEM foil (during the preliminary testing periods). The GEM foil could not be replaced due to the long time required to obtain a new foil from CERN workshop while the relay was not replaced due to the complexity of the custom made switching board.

Overall, the feasibility of using a GEM detector with segmented PCB collection plate for stopping power measurement was partially showed by the experimental work which provided similar trends to an MCNPX simulation.

This chapter provides a discussion of the most important accomplishments presented throughout this thesis and suggests possible future improvements.

The following conclusions and recommendations can be drawn from his work:

- When designing a GEM detector for alpha particle energy tracking, the range of the particle should be selected one collection segment shorter than the full length of the collection plate to ensure that the particle deposits all its energy before reaching this point. The pressure of the detector gas has to be determinate based on this required range.
- The intensity of the drift field has to be set high enough to overcome ion electron recombination from the initial ionization which can be measured experimentally by connecting the pre-amplifier to the copper electrode facing the drift region. However, setting the drift field too high leads to possible attachment of the initial electrons by the gas molecules and the signal from the initial ionizations diminishes. Moreover, the opacity of the GEM holes also increases at high drift fields as the drift field lines curve more towards the GEM copper electrode and less towards the GEM holes.
- Even though the GEM foil field should be set as high as possible to achieve high gain, reaching the maximum values is not reasonable due to the possibility of sparking between the GEM electrodes and obtaining unstable gains as the photon absorption of the quenching gas is limited. However, the high GEM gains produce more electrons that have sufficiently high energies leaving GEM to produce further ionizations in the lower fields of the induction region. Moreover, the maximum GEM voltage drop strongly depends on the gas pressure and

therefore it is highly recommended to find data that states the maximum GEM voltage for a given gas at a given pressure.

- The simulation of the induction field shows that higher induction fields are preferable for the transport of electrons towards the collection plate due to the improved direction of the field lines. Furthermore, the induction field contributes to additional electron multiplication, starting at 50% of the whole effective gain, as the electrons are still further multiplying between the GEM and induction electrode due to electrons at high energy levels leaving the GEM region. On the other hand, the increased gain created by the induction field strongly decreases the energy resolution of the detector as the electrons are multiplying over a larger distance (the thickness of the induction field) which also leads to increased fluctuations of the gain. It also contributes to increased electron attachments which subsequently lead to an increased production of negative ions, when quenching with a gas that has a large electron attachment cross section. In addition, the collection time of the negative ion is slow, and their collection time distribution deceases. At higher induction fields this could lead to the creation of noise at high count rates.
- During the construction of the detector a decrease in the levels of electronic noise was achieved by ensuring that the all the wires carrying the charge information did not come in contact with any other wires. The pre-amplifier board can also lead to the creation of high frequency noise when incorrectly grounded; the output ground (ground of the pre-amplifier output which leads to

the main amplifier) must be grounded independently of the general ground of the board. Moreover, the high voltage wires should have sufficient insulation as their can create charge build up on the insulation and create a negative pulse when discharging.

- Charge build up on a collimator is also possible when the collimator is located to close the sensitive volume electrodes. This is not necessarily visible immediately after applying high voltage to the electrodes but after some time becomes apparent by the occurrence of negative pulses.
- The power supply of the collection plate switch, like any additional electronics inside the detector, must be connected with the overall power supply of the detector, which otherwise will create electrical noise, even when the individual circuits are synchronized by connecting a common ground for the two circuits together.

## 6.1 Future Developments and Recommendations

Conclusions drawn from Chapter 5 established that the current prototype detector is not capable of measuring the stopping power of alpha particle precisely and cannot track the particle throughout its full collection region. However, the results shows that the tracking of the alpha particle is possible by this detector while applying obvious changes to the detector such as replacing the broken MOSFED relay and installing a new GEM foil. By doing so, the detector will have full capacity of tracking the heavy charge particles over the full collection plate range with wider energy spectra (mainly the lower energy deposition levels).

Moreover, a calibration technique for this device must be developed in order to obtain precise measurements from each individual collection segment due to possible shift of signal intensity over the electronic and the geometrical combination of the GEM foil and the collection segments. Such a technique could use a precise photon emitter like Fe-55, emitting photon with 5.9 KeV energy, and the commonly used gas mixture of $Ar/CO_2/CF_4$ [33], [34].

Since the constructed detector does not have assigned any particular use besides preliminary measurements and investigations of particle energy and tracking future developments are possible:

- Use of different filling gas with lower electron attachment cross section such as P-10 gas for applications when higher gains are required. For microdosimetry purposes, the detector can be filled with tissue equivalent gas.
- Improve stopping power sensitivity by replacing the current 10 segment collection plate by a higher number segment collection plate.
- Improve the scattering effect of the current collimator by the use of magnetic or electric collimator.
- Ultimately, replace the collection switch by multiple preamplifiers which will enable real time measurement of all segments at the same time.
- Replace the current charge sensitive pre-amplifier with PreShape32 chip for different particle discrimination [35], [36].

- Create a full computer simulation of the detector by combination of Garfield++ and Geant4. The Geant4 could calculate location, energy and time of created electrons from primary ionizations under a uniform electric field [37], as the drift field is relatively uniform except locations near the GEM foil. The output data would be afterwards imported in Garfield++ which would create the electron avalanche for each electron from the Geant4 simulation.

# 7 Appendix A: Example of Garfield++ Code

```
#include <iostream>
#include <fstream>
#include <cmath>
#include <iomanip>
#include <time.h>
#include <TApplication.h>
#include <TCanvas.h>
#include <TH1F.h>
#include <TGeoManager.h>
#include <TGeoMaterial.h>
#include <TGeoMedium.h>
#include <TGeoVolume.h>
#include <TGeoBBox.h>
#include <TGeoTube.h>
#include <TGeoPcon.h>
#include <TGeoHalfSpace.h>
#include <TGeoMatrix.h>
#include <TGeoCompositeShape.h>
#include "ComponentAnsys123.hh"
#include "ViewField.hh"
#include "MediumMagboltz.hh"
#include "Sensor.hh"
#include "AvalancheMicroscopic.hh"
#include "AvalancheMC.hh"
#include "Random.hh"
#include "Plotting.hh"

using namespace Garfield;
using namespace std;


int main(int argc, char * argv[]) {

  TApplication app("app", &argc, argv);
  plottingEngine.SetDefaultStyle();

  const bool debug = true;
  // Load the field map.
  ComponentElmer            *            elm            =            new
ComponentElmer("gemcell/mesh.header","gemcell/mesh.elements","gemcell/m
esh.nodes",
  "gemcell/dielectrics.dat","gemcell/gemcell.result","cm");
  elm->EnablePeriodicityX();
  elm->EnableMirrorPeriodicityY();
  elm->SetMedium(0,gas);
  elm->PrintRange();

  // Dimensions of the GEM
  const double pitch = 0.014;
```

```
const double kapton = 50.e-4;
const double metal = 5.e-4;
const double outdia = 70.e-4;
const double middia = 50.e-4;

// Setup the gas.
MediumMagboltz* gas = new MediumMagboltz();
// Specify the gas mixture (Ar/CO2 80:20)
gas->SetComposition("ar", 80., "co2", 20.);
// Set the temperature (K)
gas->SetTemperature(293.15);
// Set the pressure (Torr)
gas->SetPressure(250.);
// Set maximum electron energy
gas->SetMaxElectronEnergy(150.);
gas->EnableDebugging();
gas->Initialise();
gas->DisableDebugging();

// Set the Penning transfer efficiency.
const double rPenning = 0.51;
const double lambdaPenning = 0.;
gas->EnablePenningTransfer(rPenning, lambdaPenning, "ar");

// Load Ion mobility file
gas->LoadIonMobility("IonMobility_O-_CO2.txt");

// Associate the gas with the corresponding field map material.
const int nMaterials = elm->GetNumberOfMaterials();
for (int i = 0; i < nMaterials; ++i) {
  const double eps = elm->GetPermittivity(i);
  if (fabs(eps - 1.) < 1.e-3) elm>SetMedium(i, gas);
}
elm->PrintMaterials();

// Create files to which data will be written
ofstream outfile;
ofstream rradius;
ofstream ttime;
ofstream rratio;
ofstream ddatai;
ofstream ddatae;
outfile.open ("outfile.txt");
rradius.open ("radius.txt");
ttime.open ("time.txt");
rratio.open ("ratio.txt");
ddatai.open ("datai.txt");
ddatae.open ("datae.txt");


// Select area of interest
Sensor* sensor = new Sensor();
```

```
  sensor->AddComponent(elm);
  sensor->SetArea(-30 * pitch, -30 * pitch, -0.13,
                  30 * pitch,  30 * pitch,  0.91);

  // Selecting electron avalanche  and ion drift function
  AvalancheMicroscopic* aval = new AvalancheMicroscopic();
  aval->SetSensor(sensor);
  AvalancheMC* drift = new AvalancheMC();
  drift->SetSensor(sensor);
  drift->SetDistanceSteps(2.e-4);

  // Set number of run
  const int nEvents = 125;
  for (int i = nEvents; i--;) {
    if (debug || i % 10 == 0) std::cout << i << "/" << nEvents << "\n";
    float timeused = (float)clock()/CLOCKS_PER_SEC;
    cout<<"Avalanche " << i << "  started at " << timeused << " sec" <<
endl;

  // Set initial electron position
  double r = 0;
  double PointZ = 0.0033 + RndmUniform() * 0.9 ;
  double PointX = RndmUniform() * pitch / 2;
  double PointY = 0;
  std::cout << PointX << "\t" << PointY << "\t" << PointZ << "\n";

  // Set needed constants
  double sumElectronsTotal = 0.;
  double sumElectronsPlastic = 0.;
  double sumElectronsUpperMetal = 0.;
  double sumElectronsLowerMetal = 0.;
  double sumElectronsTransfer = 0.;
  double sumElectronsOther = 0.;
  int NII = 0;
  int NEE = 0;
  int EMUGC = 0;
  int EMLGC = 0;
  int EMIC = 0;
  int EMUG = 0;
  int EMLG = 0;
  int EMI = 0;
  int AUG = 0;
  int ALG = 0;
  int AI = 0;
  int NICG = 0;
  int NICI = 0;

    // Initial position
    double x0 = PointX;
    double y0 = PointY;
    double z0 = PointZ;
    double t0 = 0.;
```

```
    double e0 = 0.1;

    // Run electron avalanche
    aval->AvalancheElectron(x0, y0, z0, t0, e0, 0., 0., 0.);
    int ne = 0, ni = 0;
    aval->GetAvalancheSize(ne, ni);
    const int np = aval->GetNumberOfElectronEndpoints();
    double xe1, ye1, ze1, te1, e1;
    double xe2, ye2, ze2, te2, e2;
    double xi1, yi1, zi1, ti1;
    double xi2, yi2, zi2, ti2;
    int status;
    int statuss;

    // Filtrate electrons endpoints data
    for (int j = np; j--;) {
      aval->GetElectronEndpoint(j, xe1, ye1, ze1, te1, e1,
                                   xe2, ye2, ze2, te2, e2, status);
    ddatae <<xe1<< "\t" << ye1<< "\t" << ze1<< "\t" << te1<< "\t" <<
e1<< "\t" <<  xe2<< "\t" << ye2<< "\t" << ze2<< "\t" << te2<< "\t" <<
e2<< "\t" << status << "\n";

      sumElectronsTotal += 1.;
      if (ze2 > -kapton / 2. && ze2 < kapton / 2.) {
        sumElectronsPlastic += 1.;
      } else if (ze2 >= kapton / 2. && ze2 <= kapton  / 2. + metal) {
        sumElectronsUpperMetal += 1.;
      } else if (ze2 <= -kapton / 2. && ze2 >= -kapton / 2. - metal) {
        sumElectronsLowerMetal += 1.;
      } else if (ze2 < -0.129) {
        sumElectronsTransfer += 1.;
      rradius << te2 << "\n";
      NEE+= 1;
      if (ze1 > 0 && ze1 < kapton / 2. + metal) {
      // electron multiplication in upper gem collected
      EMUGC+= 1;
      }
      if (ze1 > -kapton / 2. - metal && ze1 <= 0) {
      // electron multiplication in lower gem collected
      EMLGC+= 1;
      }
      if (ze1 <= -kapton / 2. - metal && ze1 > -0.13) {
      // electron multiplication in induction collected
      EMIC+= 1;
      }
      } else {
        sumElectronsOther += 1.;
      }

      if (ze1 > 0 && ze1 < kapton / 2. + metal) {
      // electron multiplication in upper gem
      EMUG+= 1;
```

```
      }
      if (ze1 > -kapton / 2. - metal && ze1 <= 0) {
      // electron multiplication in lower gem
      EMLG+= 1;
      }
      if (ze1 <= -kapton / 2. - metal && ze1 > -0.13) {
      // electron multiplication in induction
      EMI+= 1;
      }

      if (status == -7) {
      drift->DriftIon(xe2, ye2, ze2, te2);
      drift->GetIonEndpoint(0, xi1, yi1, zi1, ti1,
                            xi2, yi2, zi2, ti2, statuss);

      ddatai << xi1 << "\t" <<  yi1 << "\t" <<  zi1 << "\t" <<  ti1 <<
"\t" <<  xi2 << "\t" <<  yi2 << "\t" <<  zi2 << "\t" <<  ti2 << "\t" <<
statuss  << "\n";
      if (zi1 > 0 && zi1 < kapton / 2. + metal) {
      //absorbtion in upper gem
      AUG+= 1;
      }
      if (zi1 > -kapton / 2. - metal && zi1 <= 0) {
      //absorbtion in lower gem
      ALG+= 1;
      }
      if (zi1 <= -kapton / 2. - metal && zi1 > -0.13) {
      // absorbtion in induction
      AI+= 1;
      }

      if (zi2 < -0.129) {
      NII+= 1;
      if (zi1 > -kapton / 2. - metal && zi1 < kapton / 2. + metal) {
      // number of ion collected from gem
      NICG+= 1;
      }
      if (zi1 <= -kapton / 2. - metal && zi1 > -0.13) {
      // number of ion collected from induction
      NICI+= 1;
      }
        ttime << ti2 << "\n";
      }
  }
  }

  outfile  <<  "\t"  <<  sumElectronsTotal  <<  "\t"  <<  "\t"  <<
sumElectronsTransfer  << "\t" << "\t" << sumElectronsOther  << "\t" <<
"\t" << sumElectronsPlastic  << "\t" << "\t" << sumElectronsUpperMetal
<< "\t" << "\t" << sumElectronsLowerMetal << "\n";
  rratio << NEE << "\t" << "\t" << NII << "\t" << "\t" << EMUGC << "\t"
<< "\t" << EMLGC << "\t" << "\t" << EMIC << "\t" << "\t" << EMUG <<
```

```
"\t" << "\t" << EMLG << "\t" << "\t" << EMI <<"\t" << "\t" << AUG <<
"\t" << "\t" <<  ALG <<"\t" << "\t" << AI << "\t" << "\t" << NICG <<
"\t" << "\t" << NICI << "\n";

  std::cout << "Event" << "\t" << "TotalE" << "\t" << "\t" << "TransE"
<< "\t" << "\t" << "OtherE"  << "\t" << "\t" << "PlastE"  << "\t" <<
"\t" << "UpMetE"  << "\t" << "\t" << "LoMetE \n";
  std::cout  << i  << "\t"  << sumElectronsTotal  << "\t"  << "\t"  <<
sumElectronsTransfer  << "\t" << "\t" << sumElectronsOther  << "\t" <<
"\t" << sumElectronsPlastic  << "\t" << "\t" << sumElectronsUpperMetal
<< "\t" << "\t" << sumElectronsLowerMetal << "\n";

  }

  // Close data files
  outfile.close();
  ttime.close();
  rradius.close();
  rratio.close ();
  ddatae.close();
  ddatai.close();


  std::cout << "    END       \n";
  app.Run(kTRUE);
```

# 8 Appendix B: Input File with Ion Mobilities

```
# ------------------------------------------------------------------
# Mobility of CO2+ ions in CO2 measured for T=30 K
# Accuracy: 7 %
# Data from Atomic Data and Nuclear Data Tables 60, 37-95 (1995)
# L.A.Viehland and E.A.Mason
# Electric Field in Td (E/N) (multiply by 250 for V)
# The negative sign in from of the drift velocity represents opposite
# direction of the velocity as the program normally consider input for
# positive ions
# E/N (10^17 V/cm^2) Vd (10^4 cm/sec)
# ------------------------------------------------------------------
# E/N   Vd
  50  -1.26
  60  -1.25
  70  -1.25
  80  -1.24
 100  -1.21
 120  -1.19
 140  -1.16
 170  -1.12
 200  -1.08
 250  -1.03
 300  -1.00
 350  -0.96
 400  -0.94
 500  -0.89
 600  -0.85
 800  -0.79
1000  -0.75
1200  -0.75
```

# 9 Appendix C: MCNPX Code For Obtaining Stopping Power Curve

```
Alpha Kinetic Energy Deposition Simulation
C ==================== Cell Cards ================================
C -------------------- Region 1 ---------------------------------
1 1 -0.00102 (15 -16 17 -18 1 -2)     imp:A=1
C -------------------- Region 2 ---------------------------------
2 2 -1.387 (15 -16 17 -18 2 -3)       imp:A=1
C -------------------- Region 3 ---------------------------------
3 3 -0.00057 (15 -16 17 -18 3 -4)     imp:A=1
4 3 -0.00057 (15 -16 17 -18 4 -5)     imp:A=1
5 3 -0.00057 (15 -16 17 -18 5 -6)     imp:A=1
6 3 -0.00057 (15 -16 17 -18 6 -7)     imp:A=1
7 3 -0.00057 (15 -16 17 -18 7 -8)     imp:A=1
8 3 -0.00057 (15 -16 17 -18 8 -9)     imp:A=1
9 3 -0.00057 (15 -16 17 -18 9 -10)    imp:A=1
10 3 -0.00057 (15 -16 17 -18 10 -11)  imp:A=1
11 3 -0.00057 (15 -16 17 -18 11 -12)  imp:A=1
12 3 -0.00057 (15 -16 17 -18 12 -13)  imp:A=1
13 3 -0.00057 (15 -16 17 -18 13 -14)  imp:A=1
C -------------------- Transport Zone ---------------------------
14 0 -19 (#1 #2 #3 #4 #5 #6 #7 #8 #9 &
   #10 #11 #12 #13)                   imp:A=1
C -------------------- External Universe ------------------------
15 0 19                               imp:A=0

C ==================== Surface Cards ==============================
C ----------------------------------------------------------------
C Planes through which alpha kinetic energy distribution is sought
C ----------------------------------------------------------------
1 py 0
2 py 0.1
3 py 0.1013
4 py 3.6013
5 py 4.1013
6 py 4.6013
7 py 5.1013
8 py 5.6013
9 py 6.1013
10 py 6.6013
11 py 7.1013
12 py 7.6013
13 py 8.1013
14 py 8.6013
C ----------------------------------------------------------------
C Bounding Planes
C ----------------------------------------------------------------
15 pz -5
16 pz 5
17 px -5
18 px 5
C ----------------------------------------------------------------
C Boundary to external universe
C ----------------------------------------------------------------
19 SO 1000
```

```
C ==================== Data Cards ================================
C -------------------- MODE Card --------------------------------
MODE A
C -------------------- Pencil Beam of Am-241 Alpha Source --------
SDEF POS = 0 -6 0 VEC = 0 1 0 DIR = 1 PAR = A ERG = 5.5
C -------------------- CUT Card for Alpha Particles --------------
CUT:A J 0.001 J J J    $Transport Alpha particles down to 1 keV
C -------------------- Material Cards ----------------------------
C Region 1 Material
m1 6000 0.01 8000 23.18 7000 75.53 18000 1.28
C Region 2 Material
m2 6000 45.45 8000 18.18 1000 36.36
C Region 3 Material
m3 18000 80 6000 6.67 8000 13.33
C -------------------- Source Intensity Card ---------------------
NPS 100000
C -------------------- PTRAC Card --------------------------------
PTRAC FILE = ASC MAX = 20000000 WRITE = ALL EVENT=SUR &
   TYPE = A
```

# 10 Appendix D: Garfield ++ Installation

## 10.1 Requirements

The Garfield++ requires the following software:

- Scientific Linux 5.X
- GCC 4.3.2 compiler
- ROOT

### 10.1.1 Scientific Linux

The Garfield++ took kit runs on 64 bit Scientific Linux 5.X only (SL 5.6 was used in this work) and can be downloaded from the link below, while it can be installed on a separate partition. It is recommended to select the AFS open client when asked to customize the software as it installs the AFS port, which could be needed in case of a GCC 4.3.2 compiler problem.

https://www.scientificlinux.org/distributions

Note, the computer graphic card should be set to "Discrete Graphics" which can be done in BIOS if the X-server (the graphical interface) does not load.

### 10.1.2 GCC 4.3.2 Compiler

#### *10.1.2.1 Option 1: Install and Download*

As the Garfield++ needs the GCC 4.3.2 compiler, which SL 5.6 does not have, and can be found in:

http://gcc.gnu.org/releases.html

The general installation guide for GCC compiler can be also found at:

http://www.faqs.org/docs/ldev/0130091154_71.htm

Since the installation might not replace the existing old GCC libraries, one can copy all files from the newly installed GCC lib64 (in our case /home/opt/gcc-4.3.2/lib 64) to the /usr/lib64/.

#### *10.1.2.2 Option 2*

The second possibility is to connect to existing gcc 4.3.2 libraries via AFS, which is significantly easier than the instantiation option but can take time and can be unstable, by copy and paste the command below. This command must br applied every time after computer shutdown or placed to "bashrc" file (/etc/) and therefore is applied automatically every single system booting.

$ . /afs/cern.ch/sw/lcg/external/gcc/4.3.2/x86_64-slc5/setup.sh

### 10.1.3 ROOT

Garfield++ is made on ROOT platform and therefore installation of ROOT is also needed. The executables can be directly downloaded from ROOT website.

http://root.cern.ch/drupal/content

The program must be set by code which can be also applied every single time or placed to “barhrc” file

$ . <directory where root folder is located>/root/bin/thisroot.sh

If program is set up correctly with the GCC 4.3.2 compiler, it should open after typing “root” anywhere in terminal

## 10.2 Installation

The installation procedure and manual is provided on Garfield++ website

http://garfieldpp.web.cern.ch

## 10.3 Running the Software

The Garfield++ code is written in C++ language, where general properties of the gas must be selected, number of run and locations of the initial (release) electrons. The electric field map is loaded from the Elmer or Ansys output files. Very clear example files for the field creation for both Elmer and Ansys can be found of the Garfield++ website. It is important to place these files within the same folder where the Garfield++ code for specific simulation is located together with any other files that the simulation should read, like mobility of ions or initial location of the releasing electrons. The example of the used Garfield++ code can be found in Appendix A together with its explanation. The simulation code must be compiled first with its makafile that can be easily downloaded from the Garfield++ website in examples and GEM simulation directory. After the C file (the file must end with .C) is converted into an executable file. It is highly recommended to obtain access to multi-core computer system or network (such as SHARCNET) due to extremely long computation times

# 11 Appendix E: Schemas of Custom Made Parts

## 11.1 Collection Plate

Dimensions are in millimetres

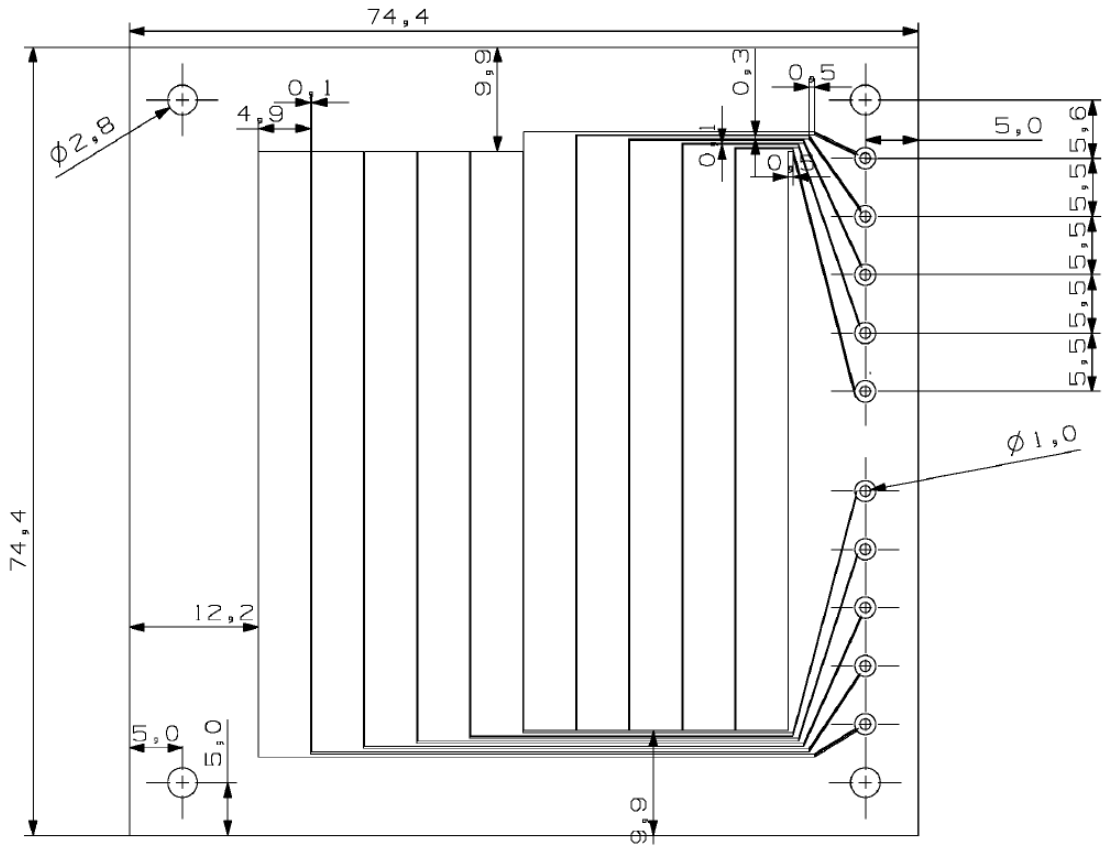

## 11.2 Drift Plate

Dimensions are in millimetres

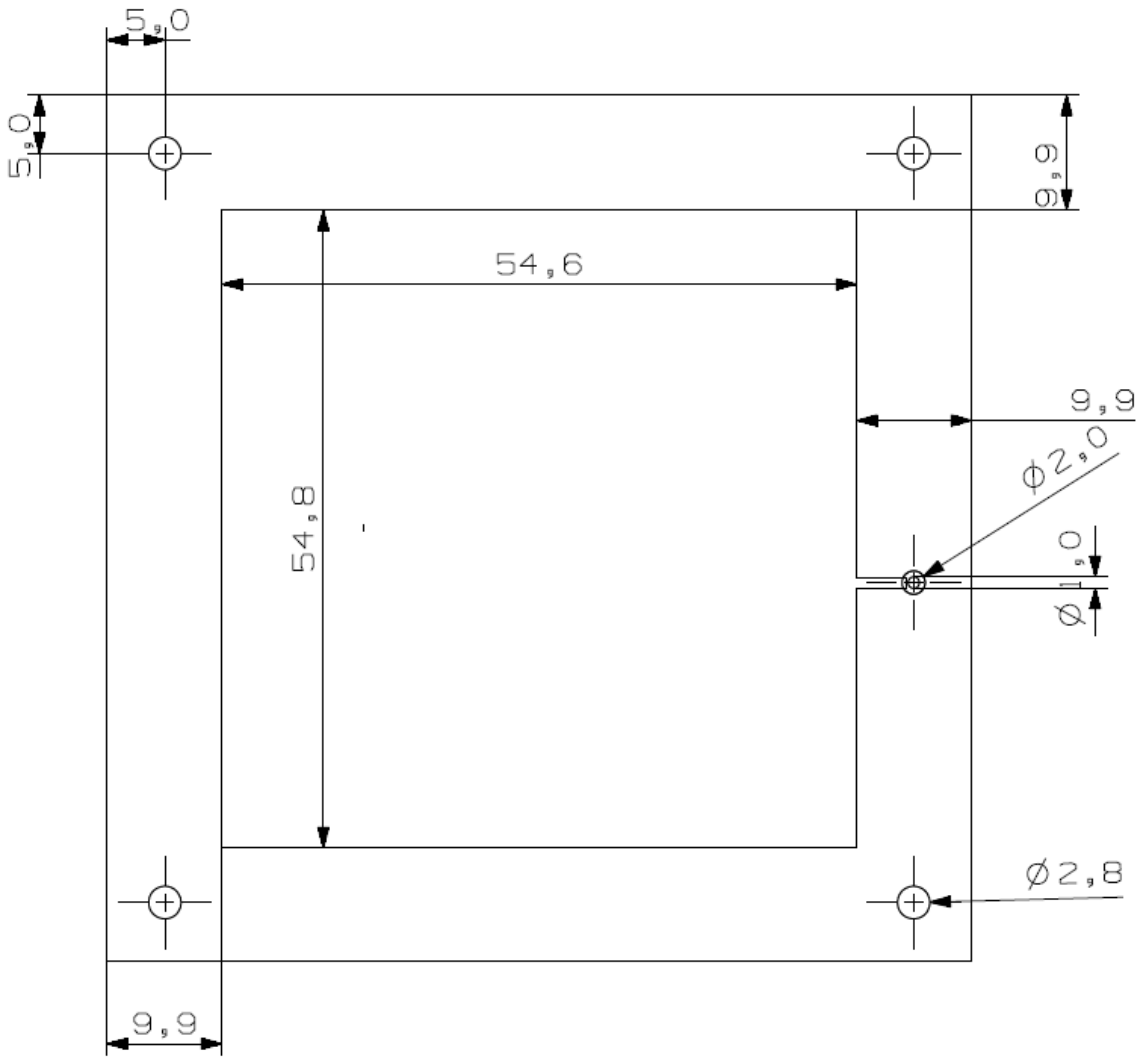

## 11.3 Collection Plate Switch Board

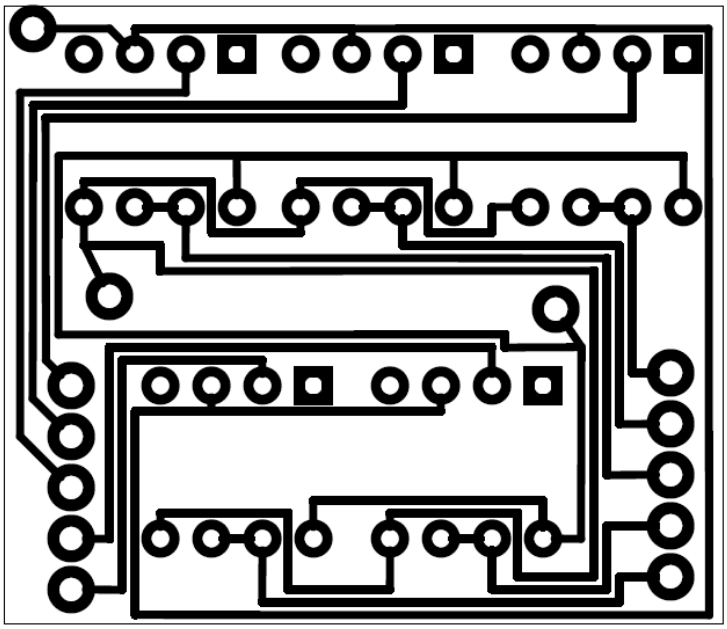

## 11.4 Connection Plate Switch Controller Board

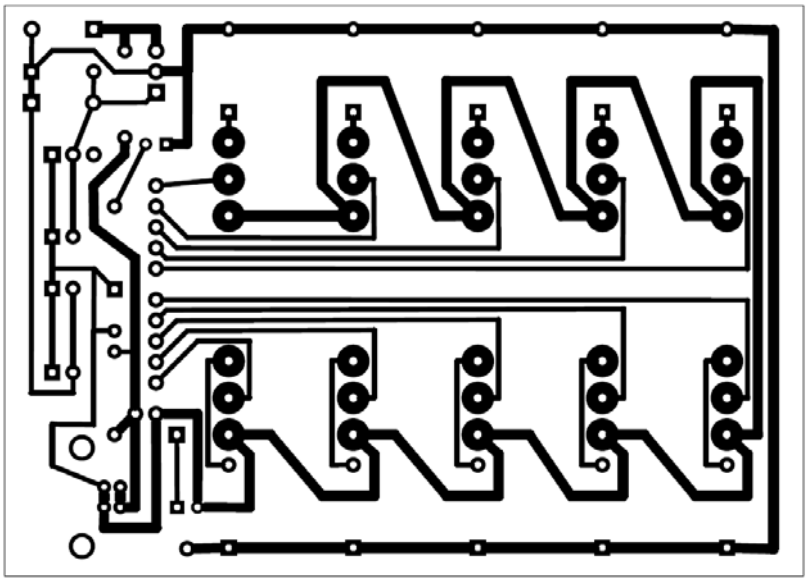

# 12 References


1. Upton, A.C. *Health Effects of Low-Level Ionizing Radiation.* 8, s.l. : Physics Today, 1991, Vol. 44.

2. Frame, P. W. *A History of Radiation Detectrion Instrumentation.* 88(6), s.l. : Health Physics, 2005.

3. Petersen, D. *Los Alamos Radiation Detectors.* 23, s.l. : Los Alamos Science, 1995.

4. Heijne, E. H.M. *Semiconductor Detectors in the Low Countries.* s.l. : Nuclear Instruments and Methods in Physics Research A, 2003, Vol. 509.

5. Frass, William. *Particle Detectors.* Michaelmas : Oxford Physics, 2009.

6. Bouclier, Roger, et al. *The Gas Electron Multiplier (GEM).* s.l. : CERN, 1996.

7. F.A.F. Fraga, L.M.S. Margato, S.T.G. Fetal, M.M.F.R. Fraga, R. Ferreira Marques, A.J.P.L. Policarpo. *Luminescence and Imaging with Gas Electron Multipliers.* s.l.: Nuclear Instruments and Methods in Physics Research A, 2003, Vol. 513.

8. Bouclier, Roger, et al. *New Observations with the Gas Electron Multiplier (GEM).* s.l. : CERN, 1997. CERN-PPE-97-032.

9. Benlloch, J M, et al. *Further Developments of the Gas Electron Multiplier (GEM).* s.l. : CERN, 1998. CERN-EP-98-050.

10. Gas Electron Myltiplier. *The Gas Detectors Development Group.* [Online] CERN. http://gdd.web.cern.ch/GDD/

11. *Polyimide Film.* Circleville : DuPont Kapton, 2012. http://www2.dupont.com/Kapton/en_US/assets/downloads/pdf/Gen_Specs.pdf

12. Hasterok, Constanze. *GEM Simulation Studies.* Dresden, : DESY, 2011.

13. U. Amaldi, W. Hajdas, S. Iliescu, N. Malakhov, J. Samarati, F. Sauli, D. Watts. *Advanced Quality Assurance for CNAO.* s.l. : Nuclear Instruments and Methods in Physics Research A, 2010, Vol. 617.

14. J. Benlloch, A. Bressan, M. Capeáns, M. Gruwé+, M. Hoch, J.C. Labbé, A. Placci, L. Ropelewski, F. Sauli. *Further Developments of the Gas.* Geneva, Switzerland :CERN, 1998, Vols. CERN-EP/98-50.

15. Knoll, Glenn F. *Radiation Detection and Measurement .* s.l. : John Wiley & Sons, Inc., 2010.

16. Chefdeville, M.A. *Development of Micromegas-like Gaseous Detectors Using a Pixel Readout Chip as Collecting.* s.l. : DARE, 2009.

17. Jamshid Soltani- Nabipour, Gheorghe Cata-Danil. *Monte Carlo Computation of the Energy Deposited by Heavy Charged Particles in Soft and Hard Tissues.* 3, s.l. : U.P.B. Sci. Bull, 2008, Vol. 70.

18. Barkas, W H. *Nuclear Research Emulsions.* s.l. : Academic Press, 1963.

19. J. Soltani-Nabipour, G. Cata-Danil. Monte Carlo Computation of the Energy Deposited by Heavy Charged Particles in Soft and Hard Tissues. *U.P.B. Sci. Bull.* Series A, 2008, Vol. 70.

20. F. Nava!, P. Vanni!, C. Lanzieri, C. Canali. Epitaxial Silicon Carbide Charge Particle Detectors. *Nuclear Instruments and Methods in Physics Research A.* 1999, Vol. 437.

21. O. Sahin et. *Penning Transfer in Argon-based Gas Mixtures.* s.l. : Journal of Instrumentation, 2010.

22. Blum, Walter, Riegler, Werner, Rolandi, Luigi. *Particle Detection with Drift Chambers.* s.l. : Springer, 2008.

23. Charge Transport in a GEM. *Garfield++.* [Online] January 2011. http://garfieldpp.web.cern.ch/garfieldpp/examples/gem/GemTransport.pdf.

24. James H. Parker, Jr. and John J. Lowke.*Theory of Eletron Diffusion Parallel to Electric Field.* s.l. : Physical Review, 1969, Vol. 181.

25. Dinner, R. Electron Attachment in Gasious Detectors. *Bachelor thesis (MIT).* 2000.

26. I. Cedaz, R.I. Hall, M. Laudau,F Pichou. Electron Attachment to Molecules and Tts Use for Molecular Spectroscopy. *Acta Chim. Slov.* 2004, Vol. 51, pp. 11-21.

27. Bondar, A. *High- and Low-pressure Operation of the Gas Electron Multiplier.* s.l. : Nuclear Instruments and Methods in Physics Research Section , Vol. 419.

28. Ö Şahina, İ Tapana, E N Özmutlua and R Veenhofb.*Penning Transfer in Argon-based Gas Mixtures.* s.l. : Journal of Instrumentation, 2010, Vol. 5.

29. H. W. Ellis, R. Y. Pa and E. W. McDaniel.*Transport Properties of Gaseous Ions over a Wide Energy Range.* s.l. : *Atomic Data and Nuclear Data Table*, 1976, Vol. 17.

30. C. D. Cooper, R. N. Compton. Electron Attachment to Cyclic Anhydrides and Related Compounds . *J. Chem. Phys.* 1973, Vol. 59, 7.

31. Bawdekar, Vaman. *Carbon Dioxide Quench Action in a Beryllium Proportional Counter*. *IEEE Transactions on Nuclear Science.* 1975, Vol. 22, 1.

32. Loeb, L. B. *Basic Processes of Gaseous Electronics.* Berkeley, CA : University of California Press, 1961.

33. Ostling, Janina. *New Efficient Detector for Radiation Therapy. Imaging using Gas Electron Multiplier.* s.l. : Department of Medical Radiation Physics. Karolinska Institutet & Stockholm University, 2006.

34. P. Colas, A. Delbart, J. Derre, I. Giomataris, F. Jeanneau, V. Lepeltier. *Electron Drift Velocity Measurements at High Electric Felds.* s.l. : Nuclear Instruments and Methods in Physics Research A, 2002, Vol. 478.

35. M. Killenberg. Lotze, A. Munnich, S. Roth, M. Weber. *Development of a GEM-based High Resolution TPC for the Internation Linear Collider.* Hamburg, : DESY, 2005.

36. Witold Matysiak, A. Hanu, A. J. Waker. *Multi-element Tissue Equivalent Proportional Counter (METEPC) for Dosimetry in Particle Therapy,* s.l. : University of Florida Proton Therapy Institute, McMaster University, *UOIT*.

37. Cortes-Giraldo, Miguel A *GEANT4 Microdosimetry Study of Ionising Radiation Effects in Digital ASIC's.*. s.l. : NUCLEAR SCIENCE and TECHNOLOGY, 2011, Vol. 2.